Amazonian Tectonic Evolution of Ceraunius and Tractus Fossae, Mars, and Implications for Local Magmatic Sources

Stephanie Shahrzad[1], Emma K. Bramham[1], Sandra Piazolo[1], Mark Thomas[1], and Paul K. Byrne[2]

[1]School of Earth and Environment, University of Leeds, UK

[2]Department of Earth and Planetary Science, Washington University in St. Louis, MO, USA.

Corresponding author: Stephanie Shahrzad (eessha@leeds.ac.uk)

Key Points:

- Three fault populations and four types of collapse features are mapped and analyzed in Ceraunius Fossae and Tractus Fossae.
- We present a 4-stage structural evolution of the area, with dike-induced deformation being the prevalent process.
- The stages of activity in the study area all occur during the Amazonian, with activity from a local magmatic source beneath Ceraunius Fossae.

Abstract

The heavily faulted Martian terrains of Ceraunius Fossae and Tractus Fossae, south of the Alba Mons volcano, have previously only been considered as parts of larger tectonic studies of Alba Mons, and the complexity of the faulting remains consequently unclear. As these terrains are in midst of the large Tharsis' volcanoes, the study of their surface deformation has the potential to help unravel the volcano-tectonic deformation history associated with the growth of Tharsis, as well as decipher details of the responsible magma-tectonic processes. In this study, we distinguish between faults and collapse structures based on image and topographic evidence of pit-crater chains. We mapped ~12,000 faults, which we grouped into 3 distinct fault groups based on orientation, morphology, and relative ages. These show a temporal evolution in the mapped fault orientations from NE to NS to NW, with associated perpendicular stress orientations. Collapse features were also mapped and categorized into 4 different groups: pit-crater chains, catenae, u-shaped troughs and chasma. Examining the 4 collapse structures reveals that they are likely 4 different steps in the erosional evolution of pit-crater chains. Together this revealed a structural history heavily influenced by both local (radial to Alba Mons, Pavonis Mons and Ascraeus Mons) and regional (Tharsis radial) lateral diking, and vertical diking from a proposed Ceraunius Fossae centred magma source. This, along with an updated crater size-frequency distribution analysis of the unit ages, reveals a highly active tectonic and magmatic environment south of Alba Mons, in the Late Amazonian.

Plain Language Summary

The large-scale faults surrounding the dome of the Alba Mons volcano on Mars has been studied intensely, while the area south of Alba Mons has not received a lot of attention. However, closer inspection of these southern terrains, namely Ceraunius Fossae and Tractus Fossae, reveals that this area is far more complex in structure and more recent in activity, than previously thought. In this study we mapped and measured all the faults in the study areas. Additional to the faults, the surface of the study area is covered in "collapse structures". These are circular to trough-like features, created when surface material has fallen into a subsurface cavity. We mapped and characterized these faults and collapse structures, in order to determine the history of events, and subsequently which geological process that created them. We found 3 distinct extensional faulting events, and examples of all 4 collapse structures: pit-crater chains, catenae, u-shaped troughs and chasmata. These events all take place within 2.4–1.4 Ga ago, during the Amazonian period.

Together, these results show magmatic activity, both from the surrounding Alba Mons, Ascraeus Mons and Pavonis Mons volcanoes, and also from a local large magmatic source, located directly underneath Ceraunius Fossae.

1 Introduction

With the advent of increasing resolution of Martian image data over the last decade, it has become possible to thoroughly investigate questions related to the tectonic regimes of Mars and determine the influence of various magmatic processes. Though larger scale processes on Mars are generally understood, more in-depth studies of more local-scale graben structures observed on Mars is incomplete. Detailed characterization of the surface structures in these local areas, and their relationships to large regional or local stress variations and magmatic processes are essential in understanding the development of the volcanic centres on Mars, and thus the evolution of the planet.

One of these volcanic centres is Alba Mons, a wide, low-relief shield volcano in the Tharsis region. The Alba Mons volcano is located on the northern edge of the Tharsis Rise has been studied in detail over the last two decades. The different surface expressions of the fault surrounding Alba Mons have been mapped; however, their interpretation differ significantly where the source of the deformation is still a matter of debate. Interpretations range from fault origin based, either purely on magmatic or tectonic processes, or combination of both (Cailleau et al., 2003a; Ivanov & Head, 2006a; Öhman & McGovern, 2014; Stubblefield, 2018). It should be noted that these Alba Mons studies focus on the northern and western faulting surrounding the main dome, leaving the southern terrains Ceraunius Fossae simplified as parts of larger studies, and Tractus Fossae often completely overlooked.

The Tharsis Volcanic province is the largest volcano-tectonic center on Mars, and is host to a myriad of individual volcanoes and their associated tectonic deformation (Bouley et al., 2016). The region of Tharsis has been in continuous development from >3.7 Ga with volcanic activity measured as recent as 200 Ma ago, during the Amazonian (Pieterek et al., 2022). The source of the extensive volcanism in the Tharsis province, has been attributed to the activity of the Tharsis superplume (E.g. Dohm et al., 2007; Mège & Masson, 1996). The superplume is considered to be emplaced underneath the entire volcanic province, consisting of several mantle plumes, and was the driving constructing factor of Tharsis from the Noachian through to the Amazonian. However, recent research has suggested that the magma source beneath Alba Mons, which would be responsible for the low-angle slope of the volcano and the extensive surface deformation surrounding it, is a separate, possibly independent plume from the Tharsis superplume (Belleguic et al., 2005; Cailleau et al., 2005; Krishnan & Kumar, 2023; Pieterek et al., 2022). This theory has its origins from the 1990 Janle and Erkul gravity study of Tharsis, which concluded that a separate diapir is responsible for Alba Mons. Common however for all these studies, is the lack of focus on the area south of Alba Mons, as most previous studies have concerned themselves with the large structures associated with the main Alba Mons dome.

In this study, we present a novel comprehensive mapping, morphological analysis and strain calculation of the faults mapped in the study areas south of Alba Mons, along with updated absolute model ages for the units. Additionally, we mapped and undertook a categorization of the observed collapse structures and determined any connections to the mapped faults. This, along with the determined likely sources of both faults and non-fault structures, was completed in order to produce a sequence of structural events, along with determining the large-and small scale tectonic and magmatic influences in shaping the surface around Alba Mons that we observe today, and thus further illuminate the magmatic and tectonic history of the Tharsis Volcanic Province, and Mars as a whole.

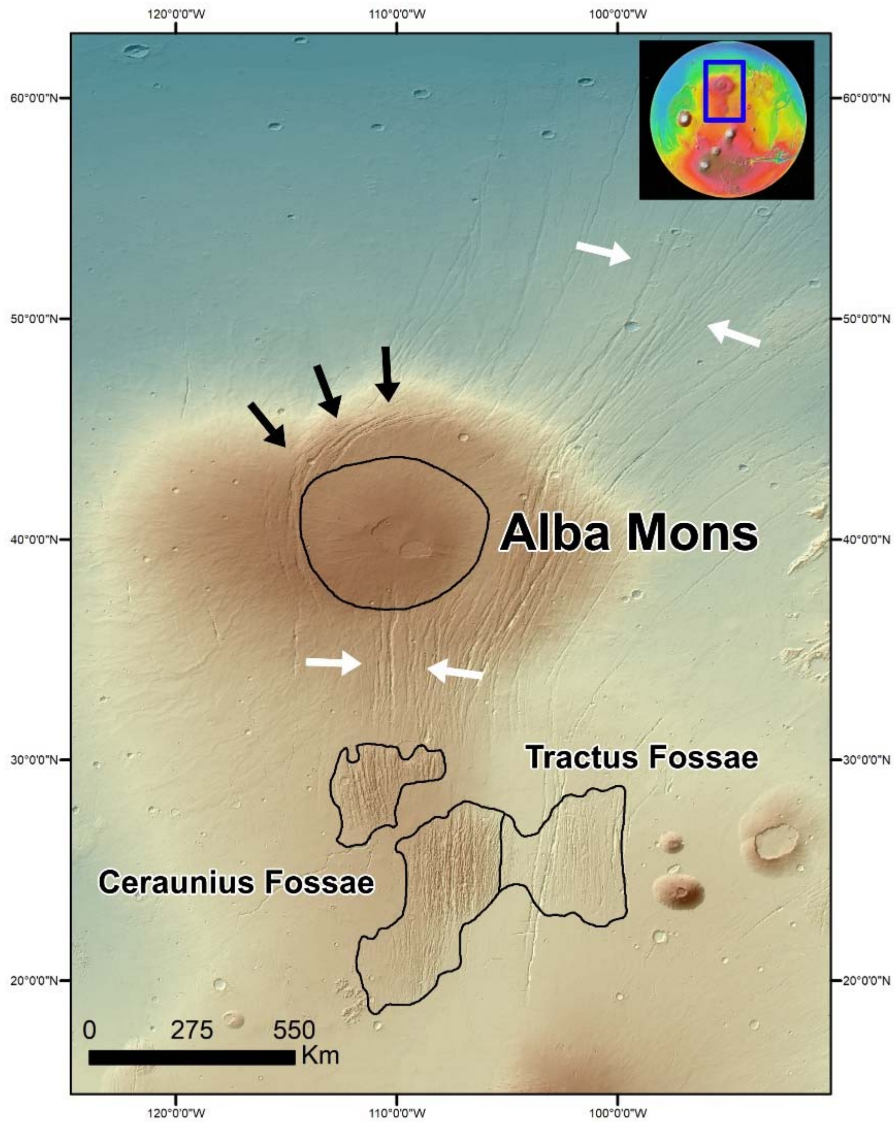

Figure 1: Location of the Alba Mons volcano (See location on top right inset of Mars). Northern white arrows indicate the Tantalus Fossae, and the black arrows indicate the Alba Fossae.

1.1.1. Morphological characteristics of the Alba Mons Volcano

Alba Mons, previously referred to as ‘Alba Patera’ has a diameter of ~1600 km, a ~7 km relief and a ~1° flank slope angle, and is such the largest edifice of any volcano on Mars (Plescia, 2004). The northern flank of Alba Mons is located proximal to the Martian dichotomy boundary, along the margin between the southern highlands and the northern lowlands (Ivanov & Head, 2006a). The summit of the volcano is host to two calderas, extensive lava flows along its flanks, and is surrounded by one of the largest graben complexes on Mars (Ivanov & Head, 2006a). The edifice itself is surrounded by Amazonian lava flows, with some topographically raised patches of older Hesperian material to the south, at Ceraunius Fossae and Tractus Fossae (Tanaka et al., 2014).

1.1.2. Graben structures associated with Alba Mons

Alba Mons is surrounded by complex graben systems, which are categorized into 3 geographical groups: Tantalus Fossae (E and NE of Alba Mons), Alba Fossae (W and N of Alba Mons) and Ceraunius Fossae (S of Alba Mons), see Figure 1 for reference. These can be subdivided further by graben structure into the following groups: (a) the north and northeast trending linear grabens and (b) concentric grabens that form the circumferential structures around the Alba Mons volcanic dome (Cailleau et al. 2003). These linear grabens bounding Alba Mons, the Tantalus Fossae, are considered the oldest, with an average strike orientation of N/NE. They are assumed to have been formed by a combination of regional stress and a broad uplift, due to a buoyancy zone underneath Alba Patera. This was reproduced in modelling studies by Cailleau et al. 2003 and Polit, et al., 2009.

Following the linear-graben formation stage, there was a temporal change to the circumferential (concentric) grabens of Alba Fossae, prevalent on the western flank of the Alba Mons volcano (Figure 1). Increasing subsidence, associated with the formation of Alba Mons, created a regime with a predominance of concentric faults in later stages of faulting (Polit et al., 2009), making the subsidence related graben-formation superimposed on the regional extension. This was also reproduced in numerical and physical models by Cailleau et al. (2003).

1.2. Collapse Features

In addition to the faults, the southern Alba Mons area has - similarly to other Martian terrains affected by volcanism - the occurrence of distinct non-fault surface features (see Figure 2 below). The morphology, location and size of these features vary significantly. These features, which we refer to as “Collapse Features”, have been described in previous literature on Mars (Hardy, 2021; Mège et al., 2002, 2003), where the definitions of pit-crater chains, catenae, u-shaped troughs, and chasmata, are described. Pit-crater chains are craters formed by a collapse, and not by an impact. These form along a chain, where material has collapsed into a subsurface void. This void can be the result of various processes, where the most widely accepted are related to tension fractures or dike-generated volatile release or magma withdrawal (Cushing et al., 2015; Ferrill et al., 2011;

Wyrick et al., 2004). The orientation of the chain reflects the collapsed structure underneath (Mège et al., 2002). Catenae is the term for a chain of pit-craters where the craters interact with each other, either doe to the initial close proximity of craters during a pit-crater chain formation event, or due to further erosion of a "standard" pit-crater chain, where the isolated craters are enhanced and thus interact. U-shaped troughs are, in this study, considered the next stage of the collapse of convalescent pit-crater chains and catenae, where collapse between individual craters results in the linear and sinuous u-shaped troughs (Mège et al., 2003). Finally, the Chasmata are generally observed as large erosional features, possibly induced by initial pit-crater chains as well, or perhaps as collapse into larger cavities than U-shaped troughs (Mège et al., 2003). However, it remains unclear exactly how these 4 collapse features are related to each other, and how they are related to the complex magma-tectonic environment on Mars.

2. Study areas: Selection, general characteristics and previous studies

2.1. Selection of study areas

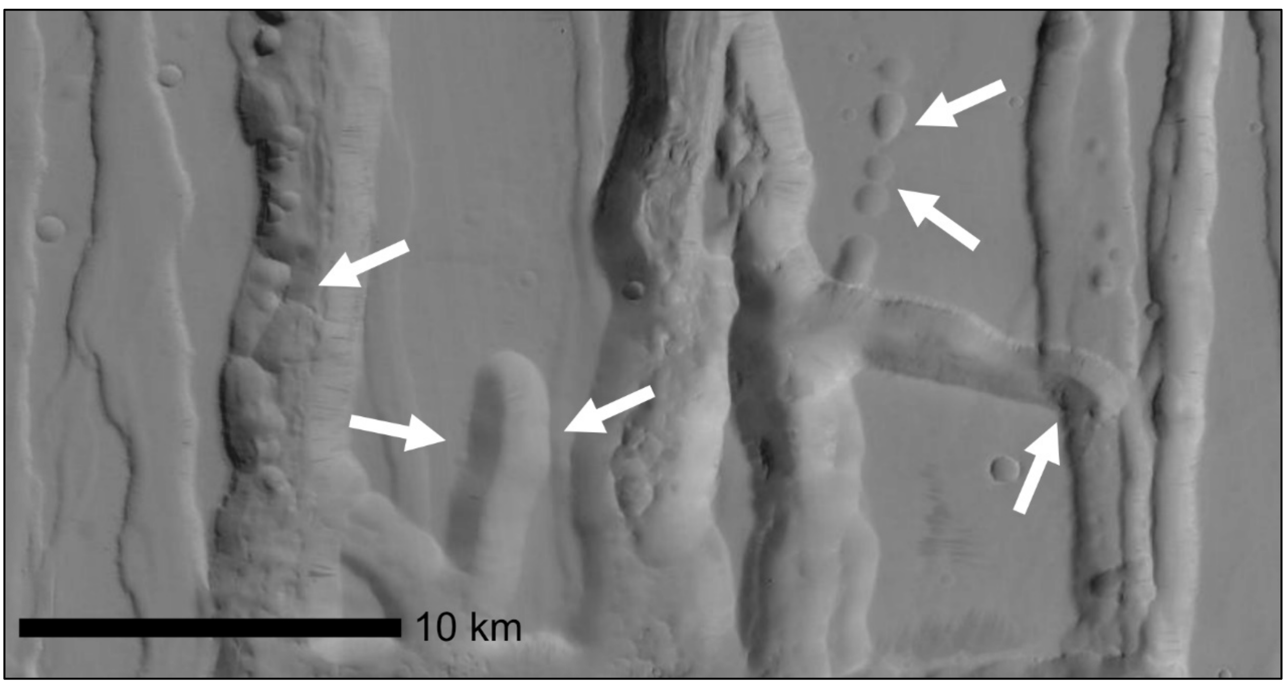

Figure 2: Zoom of example of variety of collapse structures (white arrows) found in Tractus Fossae, Mars. Background image is CTX.

The complexity of the southern Alba Mons faulting is limited within the two study areas: Ceraunius Fossae and Tractus Fossae (See Table 1 for details). Ceraunius and Tractus Fossae serve as examples of linear and curved faulting potentially related to Alba Mons, and perhaps also hosts a transition between the two types of faulting. At initial inspection, the two areas also include a number of non-graben features, with potential magmatic or volcanic origin, which we identify as the collapse features (Mège et al., 2003). Additionally, Tanaka et al. (2014) previously mapped these three areas as separate geological units, allowing for more dependable ages constrained using the crater size-frequency distribution method. As Ceraunius Fossae is divided into two units on the 2014 Tanaka map (Figure 3) with a young lava flow separating the two areas, we refer to Ceraunius North and Ceraunius South to distinguish between the two areas. Finally, these study areas have a similar distance from their nearest volcanic center (of ~600 km) as the Shahrzad et al.

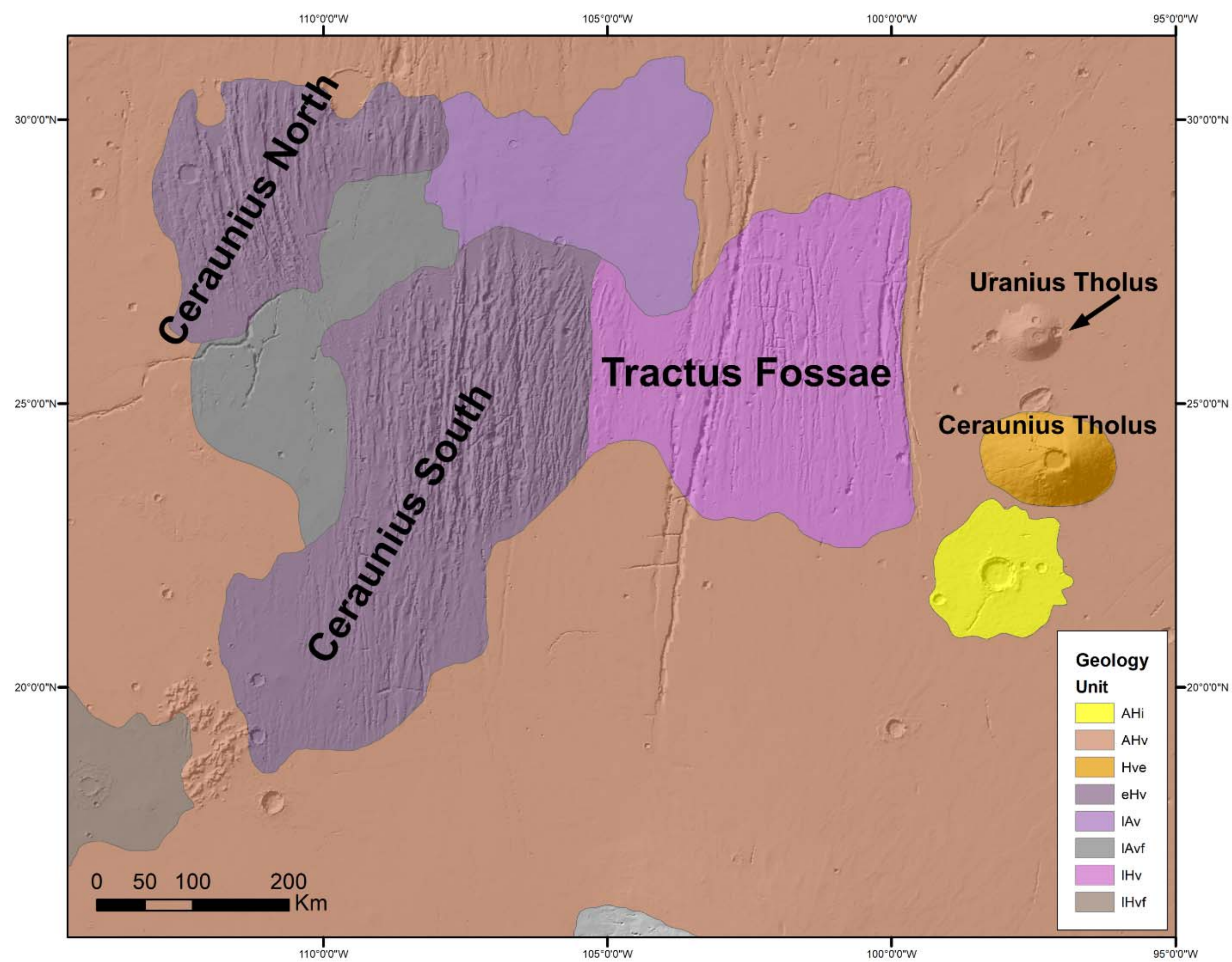

Figure 3: Geologic map of the three study areas, Ceraunius North (unit eHv), Ceraunius South (unit eHv) and Tractus Fossae (unit lHv). Geologic units from Tanaka et al. (2014)

(2023a), Ulysses Fossae fault study, which allows us to compare our Ceraunius and Tractus Fossae results to the 2023 Shahrzad et al. study, in order to broaden our understanding of the Tharsis volcanic region.

Study Area	***Unit[1]***	***Age[2]***	***Centred at[3]***	***Area Size (km²)***	***Initial observed features***
Ceraunius North	eHv	3.65 Ga	111° W, 29° N	42,746.9	Linear fault, curved faults, collapse structures
Ceraunius South	eHv	3.65 Ga	107° W, 23° N	112,434.75	Linear faults, curved faults, collapse structures
Tractus Fossae	lHv	3.55 Ga	101° W, 25° N	82,260.60	Linear faults, collapse structures

Table 1: Summary of study areas. [1,2] Unit and Age as defined by Tanaka, 2014. [3]As determined on Google Earth, Mars.

2.2. General characteristics and previous studies

2.2.1. *Ceraunius Fossae North and South*

The faulted terrain immediately to the south of the Alba Mons shield, is a part of the *Ceraunius Fossae* system (Figure 3). These linear faults appear to be oriented generally north-south, largely radial to the Alba Mons shield. The Ceraunius Fossae fault system is composed of two raised patches of fault and graben systems, which are separated by lower-elevation, younger lava flows, effectively preserving a significant larger number of structural features than that of the surrounded flooded plains. Previous work by Tanaka (1990), determined a two-stage sequence of faulting in the area, with an initial NE and then NS oriented extensional events. For the purpose of this study, the two patches of Ceraunius Fossae faults are divided into the two areas shown on Figure 3, Ceraunius North and Ceraunius South. In this study we define these areas as within the boundaries mapped by Tanaka et al. (2014), where both the units are mapped within the early Hesperian volcanic unit (eHv), with an absolute model age of 3.65 Ga (Table 1) (Tanaka et al., 2014).

2.2.2. *Tractus Fossae*

Tractus Fossae is located immediately to the east of Ceraunius Fossae, and consists of its own unit, mapped by Tanaka et al. (2014) as lHv, the *late Hesperian volcanic unit.* This unit is aged 3.55 Ga (Tanaka et al., 2014), and is thus considered the youngest of the three study areas. Immediately to the east of the area, the two smaller volcanoes Uranius Tholus and Ceraunius Tholus are located, with diameters of ~60 km and ~130 km, respectively (Figure 1). Tractus is similarly faulted with large linear grabens, though they appear more spread out than the Ceraunius Fossae faults. Tractus is also host to two very large linear structures along its western border, with Tractus Catenae being the only named one, which appear to be longer and deeper than the other faults in the area. This particular area has only one dedicated study by Spagnuolo et al. (2008), who identified the faulting in Tractus Fossae to being as early as the Noachian-Hesperian boundary, followed by some faulting in the Amazonian.

The thousands of faults with lengths of hundreds of kilometres, and with varying orientations, have been examined largely with the full scale of Alba Mons' deformation, an area which covers more than 2,000,000 km^3. In this study, we chose representative areas of the main linear and curved structures and took an in-depth look at the faults and collapse structures on the surface, in order to refine the structural evolution of the northern section of the Tharsis Volcanic Province and determine the role of Alba Mons in their development. Here, we map and categorize the extensive overprinted fault systems along with any collapse features, located to the south of the Alba Mons edifice. Additionally, we mapped the location and size of these collapse features in ArcMap and categorized them. We examined their morphology, in order to categorize their appearance and location into the 4 collapse variations mentioned above. This was done in order to determine the conditions that would cause the collapse features to form, in order to use them as potential indicators for the immediate endogenic environments. This, along with the determined likely sources of both faults and collapse structures, was completed in order to produce a sequence of structural events, along with determining the large and small scale tectonic and magmatic influences in shaping the surface around Alba Mons that we observe today.

2 Methods

2.1. Fault characterization

2.1.1. Fault mapping and grouping

We mapped the faults in this study using 6 m/pixel resolution global image mosaics from the Mars Reconnaissance Orbiter's Context Camera (CTX) (Malin et al., 2007). We mapped the fault traces as separate polylines using ArcMap software, at a scale of 1:250,000 to 1:100,00, where we traced the upper boundary of the fault (surface breaks), identified by the change in slope visible on the images. For our 3 study areas of Ceraunius North, Ceraunius South and Tractus Fossae, we used the Tanaka et al. (2014) geologic map as unit boundaries and mapped the faults within. Any fault that started within the defined study area boundary, was mapped in full even if the trace continued beyond the boundary. We aimed to map all identifiable faults at the chosen scale, in order to capture each fault trend, in order to reduce bias. For fault length determinations, we only considered any fault linkage visible on the surface (hard-linked faults), and we have not made any conjectures regarding supposed sub-surface linkage of potentially soft-linked faults. The absolute lengths and strike orientations were calculated as geodesic lengths and azimuths using the Tools for Graphics and Shapes plugin for ArcGIS (Jenness, 2011). We used the software package FracPaQ (Healy et al., 2017), to visualize fault strikes spatially and in rose diagrams, along with the mapped fault intensity. In FracPaQ fault intensity (m^{-1}) is determined by the number of faults intersecting the perimeter of a program generated scan circle (Healy et al., 2017). In this study we used a grid comprising of circles with a diameter of ~10 km, to ensure capturing the complexity of the faulting in the area.

Following the fault mapping, we separated the mapped faults into different fault groups defined by similar average orientation (as calculated in FracPaQ), fault morphology, relative ages determined by their crosscutting relationships. This subsequently ensured that the faults within a group are all of similar ages and are therefore inferred to have formed through the same structural event.

2.1.2. Expected observations for faulting driven by intrusions or pure tectonic deformation.

For intrusion initiated faulting we are looking for grabens that have a uniform width, depth and lengths (Tanaka et al., 1991). These are generally narrow and symmetrical linear relief ridges

(Mège, 1999), with a radial or fan-shaped fault population geometry, extending from a volcanic source (Carr, 1974; Mège & Masson, 1996). These are also often associated with other linear surface features such as pit-crater chains, chasmata and u-shaped troughs (Mège & Masson, 1996). For purely tectonic extensional faulting, we expect a less narrow shaped graben, with less symmetrical and more irregular spatial fault patterns within a population. In terms of geometry, grabens associated with volcanic loading, uplift or subsidence will show circumferential, wristwatch or hourglass patterns (Byrne et al., 2015; Cailleau et al., 2003a, 2005). Non-volcanic tectonism such as flexural loading, uplift or isostatic compensation will generally either be accompanied by radial or circumferential wrinkle ridges (compression) (Banerdt et al., 1992; Tanaka et al., 1991).

2.1.3. Strain measurements for faults

The strain for each defined fault group was measured using sets of topographic profiles, created perpendicular to the main fault orientation in each group. The topographic profiles were generated in QGIS software, where we used data from the blended MOLA and HRSC DEM. The location of each topographic profiles was determined by the criteria of being perpendicular to the average fault orientation within a group and was created so the trace would not cross any other major topographic features, such as craters, while still capturing as many faults as possible. This process was somewhat limited by the availability of data in the DEM quality of certain areas.

We measured the extensional strain (ϵ) by calculating the sum of measured throws (Shahrzad et al., 2023a) and used a 60° fault dip (consistent with previous Martian estimations (Polit et al., 2009)), to calculate the cumulated extension (e_{cum}). This was then divided by the original length of the profile trace (L_0), defined as the trace length minus the sum of the heaves.

$$\epsilon = \frac{e_{cum}}{L_0}$$

We then multiply the result with 100 to get the strain percent value.

2.2. Collapse Feature Mapping

The collapse features in the three study areas were similarly mapped by marking each feature with a polyline in ArcMap, which went through the middle of the feature, recording their location and orientation. The four collapse features were identified during the mapping as follows:

Pit crater chains and catenae were the easiest to identify, as the craters make them non-ambiguous. These features are straightforward to identify on the CTX images alone, where the distinction from individual pit craters to catenae is determined by when the craters touch or directly interact with each other, while the individual craters are still identifiable.

U-shaped troughs were more difficult to distinguish from the tectonic grabens, as they have largely similar straight linear borders. They do however vary from the grabens by several features: 1) uneven border walls, with some indications of remnant circular crater perimeter features (scalloped edges). 2) Contrary to the tectonic faults which remain parallel through their trace, the troughs terminate in a semi-circular shape where the walls connect. As the U-shaped troughs can be a challenge to distinguish, the mapping of them is aided by comparing the CTX images with the topographic data. For topography we used the global Digital Elevation Model (DEM) from the Mars Orbiter Laser Altimeter (MOLA) data and the High-Resolution Stereo Camera (HRSC) (Fergason, R. L. et al., 2018). The DEM data has a vertical resolution of 1 m/px and a horizontal resolution of 463 m/pixel (Fergason, R. L. et al., 2018). As we determine u-shaped troughs as a stage in evolution of the pit-crater chains, the majority of the troughs reveal distinct pit crater chains beneath them on the topographic data, distinguishing them from the purely tectonic faults.

The final collapse feature, *chasmata,* can appear similar to U-shaped troughs but are larger in size (Mège et al., 2003). They often bounded by faults, with interiors that show evidence of large-scale mass wasting, with slopes of material along the sides, distinguishing them from the defined slope breaks of the purely tectonic faults. They commonly form large oval structures. After mapping each feature, the orientation and length of the features was measured using the Graphics and Shapes tool in ArcMap.

2.3. Determining relative and absolute ages

We determine the timing of the activity of the different defined fault groups as constrained by their absolute maximum ages and their relative ages. The maximum absolute ages were determined by the age of the geological unit the fault groups crosscut, which we determined in this study using crater size-frequency distribution. The vast majority of the fault groups in this study crosscut multiple geological units, and in these cases, we assigned the youngest unit age as the maximum age for the group. The relative ages of the fault groups themselves, were identified through their cross-cutting relationships.

2.3.1. Crater size-frequency distribution

We obtained absolute model ages for the geological units of the three study areas (Figure 3), using the crater size-frequency distribution (CSFD) method, with a similar approach as the Shahrzad et al. (2023a) study. We mapped all identifiable craters which had a diameter >800m, with the aim of using all mapped craters ≥1km in the age determination. This mapping of smaller diameters than the aim, ensured that no craters ≥1km was missed. The crater sizes and locations were mapped in ArcMap using the CraterTools plugin (Kneissl et al., 2011). During mapping we ensured no capturing of secondary craters (clustering) or other circular features that may have been mistaken for a primary impact crater, such as pit-crater chains. We used the software Craterstats v.2 (Michael, 2013) to fit our crater data to the Martian isochrons, using the production function of Hartmann (2005) and the chronology function of Hartmann and Daubar (2016). The counted craters were then fit with a lower diameter boundary of 1 km.

3 Results

3.1. Fault mapping

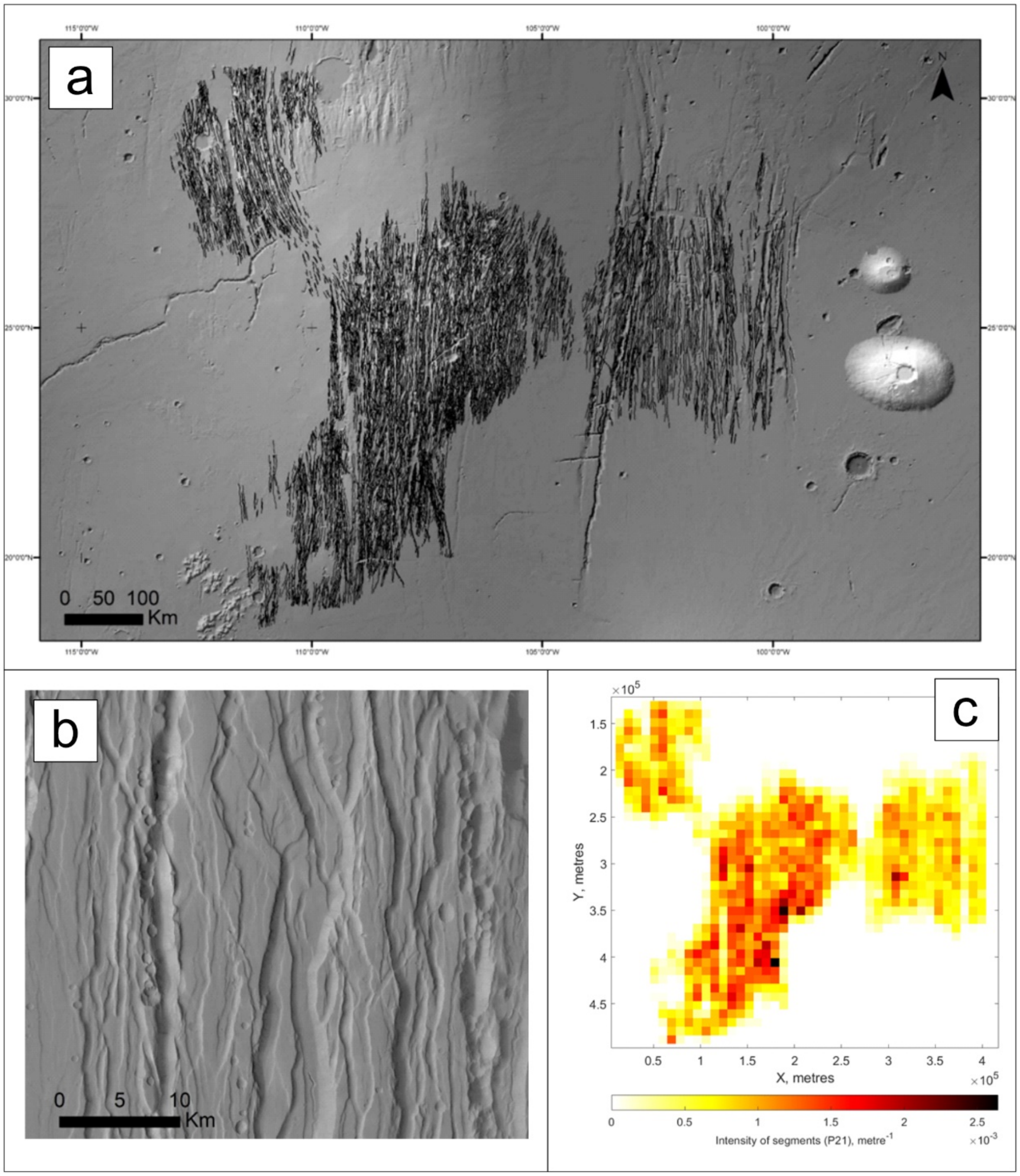

Figure 4: A) All mapped faults (black lines) in the study area. Background image is MOLA Hillshade. B) Zoom on example of overprinted fault patterns. C) Fault intensity map of mapped faults.

We mapped a total of ~12,000 faults in the south of Alba Mons (see Figure 4a), across the three study area units, the vast majority of which are graben-forming normal faults which have an average strike orientation between NNW and NNE. The faults heavily overprint each other (Figure 4b), and have a largely similar appearance and morphology. The majority of the graben are linear, but there is a number of faults with variations in orientation along strike, with some of them being subtly curved, e.g., the eastern faults in Ceraunius North (Figure 4a). We have mapped a cumulative length of 106,516,6 km of faults, with the average fault length being ~8 km. Among the three geological units, the fault intensity map revealed a relatively even spatial distribution between the two flanking units Ceraunius North and Tractus Fossae, with the middle Ceraunius South unit having the highest intensity of faulting (Figure 4c). Common for all the grabens mapped, is the consistent width across strike, which is constantly a few km (2-4 km), resulting in relatively narrow grabens when considering their lengths.

3.1.1. Fault groups

The initial approach of dividing the faults into groups based on cross-cutting relationships alone proved difficult, due to the highly overprinted nature of the faulting (Figure 4b). This was particularly true for the NS oriented faults in Ceraunius South, where it was challenging to distinguish if faults were changing orientation along strike within a group, or if a fault should belong to an entirely different group with a different average orientation. To allow a more detailed and consistent identification of fault groups, we expand on our initial method. We used the general N-S orientation of the majority of the faults as the baseline for the first group, and then systematically marked any individual fault which 1) had a discernibly different average strike orientation from the N-S group (see rose diagrams in Figure 5) and which 2) crossed the N-S fault independently and was clearly not a branch from the NS fault orientation group. This left us with 2 initial fault groups, the N-S group, and a second group of faults that did not belong in the N-S group. We then analysed the second group and used our original criteria of clear cross-cutting relationships and different strike orientation, to further divide that group into two groups, conclusively resulting in 3 final fault group in our study area (Table 2). See Figure 5 for the groups.

Fault Group	(N) Faults	Cumulative Length (km)	Avg. Orientation	Unit
G1	1676	13,061	NNE/NE	CS, TF
G2	8013	76,213	N/NNE	CN, CS, TF
G3	2242	17240.7	NNW/NW	CN, CS

Table 2: Overview of the 3 fault groups. Which units the faults in the group superpose: CN (Ceraunius North), CS (Ceraunius South), TF (Tractus Fossae).

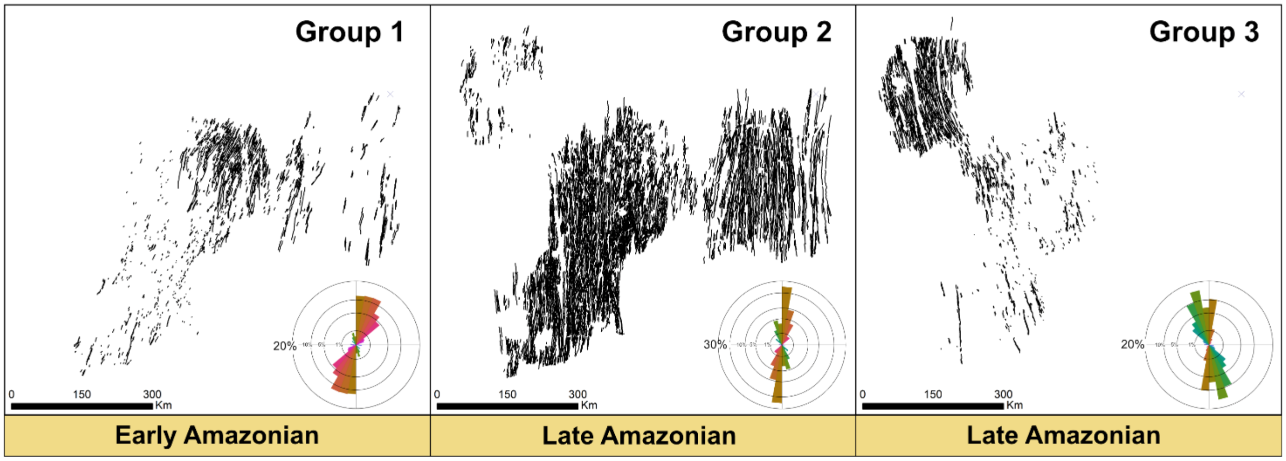

Figure 5: The three fault groups identified in Ceraunius Fossae and Tractus Fossae, with main fault orientations showed in the rose-diagrams.

Group 1 is a relatively sparse group of faults, which crosscut the Tractus Fossae and Ceraunius South units. The main strike orientation is towards NNE, with some subtly curved faults within the Ceraunius South section of faults, which start with a NNE orientation, and then curves more towards the NE, the further north the trace goes. The faults in Group 1 have very few interactions with the Group 3 faults, so we therefore use the Group 2 faults to determine relative ages. In places where the two groups interact, the faults in Group 1 are consistently crosscut by the faults in Group 2, making the Group 1 faults the oldest of the two groups.

Group 2 consists of faults with a largely N-S orientation, and the majority of them (the Ceraunius South faults) are radial to the main Alba Mons edifice. The faults in this group are mostly linear, but due to heavy overprinting, the faults appear to braid or branch in between each other (see Figure 4b). The faults are largely contained within the unit boundaries, but Group 2 the only group with faults which crosscuts all three study areas, and thus interacts with the two other fault groups. It is by far the most populous group, containing ~70% of all the mapped faults.

The faults in Group 3 appear to crosscut the faults in Group 2 and are therefore the youngest of the three groups. These faults appear only on Ceraunius North and Ceraunius South and have almost no interactions with Group 1. However, similar to Group 1, a portion of faults in this group are also curved, though their orientation is mirrored from Group 1. In Group 3, the curved faults, which are located in the eastern part of Ceraunius North, are curving from a NW to NNW orientation, the more north the fault trace appears. The linear faults in the south and west maintain a NNW orientation through strike. The faults in Group 3 also shows two very wide graben features, where the largest normal fault-bounding graben is ~ 10 km in width.

3.2. Strain

We measured the strain across all 3 defined fault groups, and determined maximum strains of 2%, 3.2% and 2.3% for Groups 1, 2 and 3 respectively. As both Groups 1 and 3 had a comparable number of faults (Table 2), with the faults spread over a largely similar area, the resemblance in strain % is not surprising. The strains for Group 2 are the highest, corresponding with the largest number of faults.

3.3. Absolute Ages

We determined the ages of the three units in Ceraunius Fossae and Tractus using CSFD and plotted the ages in Craterstats v.2. The crater data was constrained using a 4t^{h} root-2 binning, and a Poisson distribution fit (Michael et al., 2016). These mapped craters resulted in three Amazonian ages for the units, with Ceraunius North exhibiting a much younger age than the other two units, see Table 3 below. An example of the CSFD plots for Ceraunius South are shown in Figure 6 below. See Figure S1 in the Supporting Information for all 3 CSFD plots.

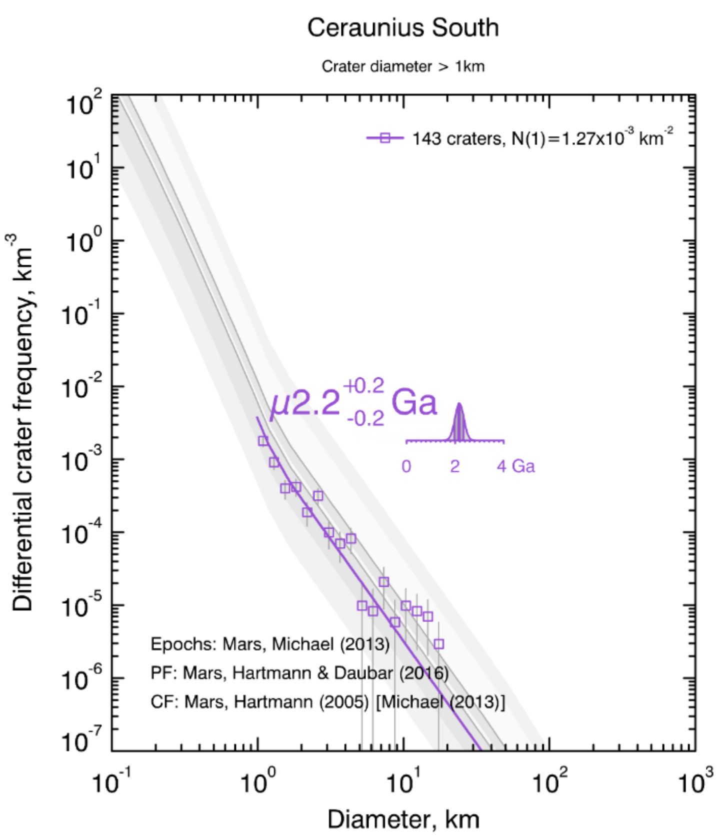

Figure 6: Crater Size-Frequency distribution (CSFD) plot for Ceraunius South, showing a best fit age of 2.2 Ga.

Area Name	**Unit name***	**(N) Craters >1km**	**Unit age**	**Period**
Ceraunius North	*Early Hesperian volcanic unit (eHv)*	34	1.4 ± 0.2 Ga	Late Amazonian
Ceraunius South	*Early Hesperian volcanic unit (eHv)*	143	2.2 ± 0.2 Ga	Early Amazonian
Tractus	*Late Hesperian volcanic unit (lHv)*	115	2.4 ± 0.2 Ga	Early Amazonian

Table 3: Overview of absolute model ages of the 3 study areas (Figure 3).

These results all suggest a maximum age for the mapped faulting in Ceraunius Fossae to be Amazonian, with the oldest material being Early Amazonian. This is the case for the faults in Group 1, which crosscuts both Ceraunius South and Tractus Fossae, but not Ceraunius North. Due to the group being crosscut by Group 2 which is then crosscut by Group 3, we determine the Group 1 faults as the oldest of the mapped faults. Group 1 is then chronologically followed by Group 2 and then Group 3, where both groups are cross cutting the youngest unit, Ceraunius North, which has a Late Amazonian age of 1.4 Ga (see Table 3). For Group 1 and 3, the southern section of faults is highly fragmented, and shorter than their northern faults of similar orientation. We attribute this to the highly overprinting of faults, where the high intensity faulting (Figure 4b) is obscuring the actual fault traces of any not NS oriented faults.

3.4. Collapse structures

During our mapping we came across 4 distinct types of collapse features, as described in the methods section. These were mapped separately, and we present an overview of the structures below on Figure 7:

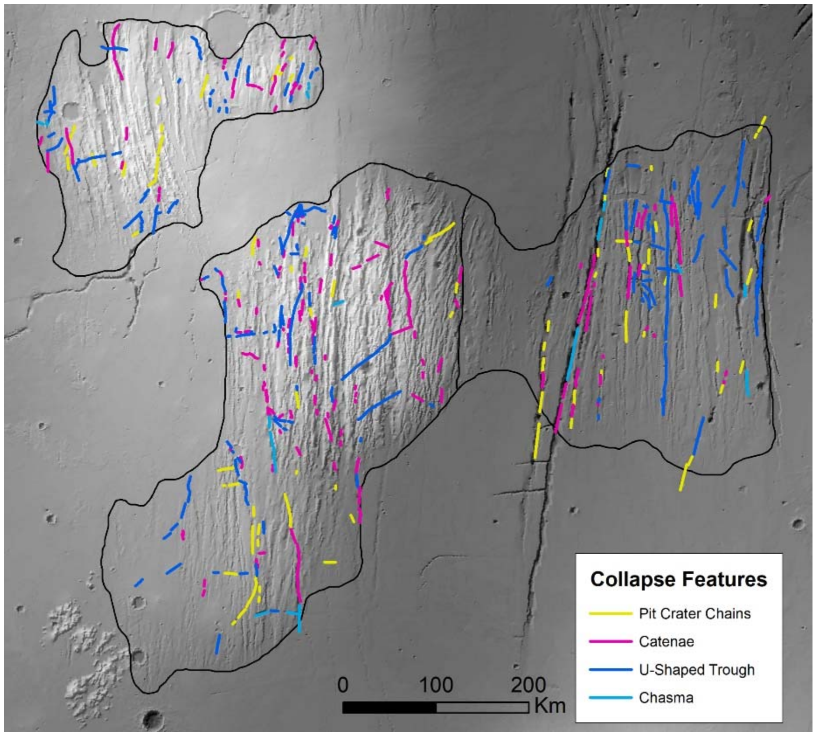

Figure 7: Location of mapped collapse features in the three study areas.

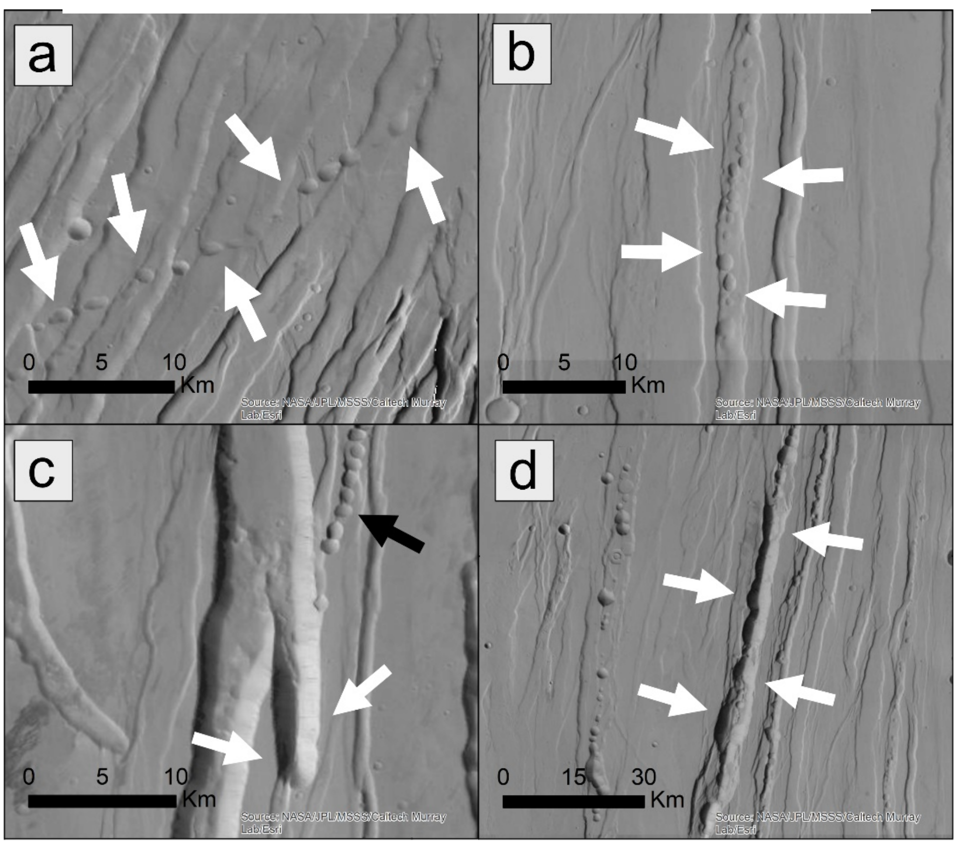

Figure 8: Example of a) independent pit-crater chains (Type 1) and b) a pit-crater chain located between two faults (Type 2). C) U-shaped trough example (white arrows). The black arrow shows a pit-crater chain. d) Example of chasmata in Tractus Fossae (white arrows). Background image CTX

Pit-crater chains and Catenae

The first abundant features found in the Ceraunius Fossae and Tractus Fossae area, are pit-crater chains and catenae. Both pit-crater chains and catenae are found amongst the majority of fault groups and are either dotted through the landscape independently from the faults or are located nested in between two graben-bounding faults (Figure 8a and 8b). A portion of the pit-crater chains which are located within grabens, show fault driven formation characteristics (e.g., en echelon distribution along strike, asymmetric pits etc.). These chains are largely following the N-S orientation of the majority of the faults in Group 2, however there are instances of short pit-crater chains, with an N-E orientation.

U-shaped Troughs.

U-shaped troughs appear as linear troughs, or as branches from the large graben-forming faults, where they are usually formed perpendicular to the main fault strike orientation. These features are found on all three study areas, but their large striking and complex appearance is the most evident in Tractus Fossae

Chasmata

Another feature found in our study areas are chasmata, which appear as a combination between the pit-crater chains and the u-shaped throughs with their sharp but circular edges (Figure 9c). These are generally the largest features of the four identified and can be up to 70 km long and is found on all three study areas (Table 4).

These collapse features are all observed within narrow grabens, positioned parallel to narrow grabens, or perpendicular to narrow grabens. This is especially true for the pit crater chains which occasionally do not follow the orientation of the grabens. In cases where the independent pit crater chains and the grabens interact, the crosscutting relationships always suggest that the pit crater chains are younger, though the time span between the two are undefined.

Table 4: Overview of mapped collapse features.

Feature name	Number of features	Prevalent Orientations	Cumm. length	Average length	Characteristics
Pit-Crater Chains	81	N-S/NNE	895.3 km	11.1 km	• Separate craters in chain • Majority located within grabens, with some independent chains.
Catenae	168	N-S/NNE	1625.7 km	9.4 km	• Crater chain, with craters interacting with each other.
U-shaped Trough	181	N-S/NE/E-W	2263.3 km	12.4 km	• Non-tectonic troughs. • Show underlying pit-crater chains in topographic data.
Chasmata	17	N-S/E-W	272.2 km	16 km	• Large mass-wasting chasms, often oval shaped.

4 Discussion

4.1. Determining the fault groups

Fault mapping in our three study areas revealed a series of highly dense graben formations (Figure 4C), facilitated by extensional faulting. The faults are predominantly linear (Figure 5), though the northern section of Ceraunius North and Ceraunius South hosts faults which exhibit a slight curvature, their shape suggesting a different extensional environment from the linear faults. The 3 fault groups were straightforward to distinguish, except for the southern section of Ceraunius South. Here, the intense overprinted fault pattern made it challenging to discern individual fault traces, which may be why the mapped faults in this region are relatively fragmented and short compared to the rest of the more cohesive mapped faults (Figure 5). Results from our work agrees with previous studies (Cailleau et al., 2005; Tanaka, 1990), in that the first stage of faulting consist of the NE striking faults, followed by a NS oriented graben formation. We also define a third stage of activity, younger than the NE and NS orientations, with our Group 3 NW oriented faults.

Group 1 faults have a primary orientation of NE. However, some of these faults start with a more NS trace from the south, and change orientation towards the NE, when the faults approach the main Alba Mons shield (Figure 5). Group 2 faults, which form the linear NS grabens, are radial to both the Alba Mons and Tharsis centres, making it difficult to assign a source of this E-W stress field based on orientation alone. Group 3 faults are slightly dissimilar to the Group 1 and 2 faults, in that the grabens are wider, and the majority of the faults are curved.

4.1.1. The Young Ages of Ceraunius and Tractus Fossae.

The absolute model ages calculated in this study using crater size-frequency distributions (CSFD) on the three study area units, all resulted in young Amazonian ages. This makes Ceraunius North 1 Ga younger than the other two units, and all three study areas 1-2 Ga younger than the previously mapped 2014 Tanaka et al. ages (Table 5).

Table 5: Comparison of previous (Tanaka et al., 2014) CSFD ages, and the ones calculated in this study (Unit age).

Area Name	Unit name	Prev. age	Unit age	Period
Ceraunius North	*eHv*	3.65 Ga	1.4 ± 0.2 Ga	Late Amazonian
Ceraunius South	*eHv*	3.65 Ga	2.2 ± 0.2 Ga	Early Amazonian
Tractus Fossae	*lHv*	3.55 Ga	2.4 ± 0.2 Ga	Early Amazonian

Similar to the young Ulysses Fossae ages found in Shahrzad et al. 2023a, our CSFD study of southern Alba Mons is a part of a significantly more detailed study of the craters in this specific area, when compared to the most recent global Tanaka 2014 study ages (Table 5). The higher number of data points in our study enables more specific statistics, to specify the ages of the units, which has expectedly decreased the previous ages (Table 5). The 1.4 Ga age for Ceraunius North is however an outlier, and we considered the possibility of flooded craters potentially artificially lowering the age of Ceraunius North. However, after considering the morphology of the mapped craters, we did not observe sufficient evidence to attribute the exceptionally young unit age to flooded craters alone, though it remains a definite possibility. Considering the appearance of the 3 study areas, Ceraunius North has fewer faults and graben in total as a result of its smaller area size, but the young age found in the results is not reflected in the appearance of the grabens, which are similar to the two other study areas.

Regarding the young Amazonian ages for all the study areas, studies on low shields, lava flows and volcanic edifices in Ceraunius Fossae have revealed that late Amazonian (<200 Ma) volcanic activity occurred in the Ceraunius Fossae region (Christoph & Garry, 2017; Krishnan & Kumar, 2023; Pieterek et al., 2022). Studies by Ivanov & Head (2006) and more recently Krishnan &

Kumar (2023) also looked at the Ceraunius Fossae grabens, as part of larger studies of the Alba Mons area. The former study determined a late Hesperian to early Amazonian graben formation of the radial faults in Ceraunius Fossae (Ivanov & Head, 2006a). The Krishnan & Kumar (2023) study found absolute maximum graben ages for 54 select grabens in Ceraunius Fossae to be Amazonian. 63% of those grabens were determined to be late Amazonian in age, where some grabens are younger than 100 Ma (Krishnan & Kumar, 2023). These results favourable towards our arguments of Amazonian fault activity in Ceraunius Fossae and has implications for the ages of active volcanic and magmatic processes.

4.2. Fault formation mechanism

With defined groups and ages, we examine the morphology and appropriate stress fields which would be responsible for the orientation of the faults, in order to evaluate the sources of the mapped faults. The mapped orientations of the faults seem to suggest 3 distinct and different stress fields, one responsible for the 3 different orientations of faults in Ceraunius North, Ceraunius South and Tractus Fossae (Figure 5). The morphology of the faults in Group 1, 2, and the linear faults in Group 3 (i.e., narrow grabens, uniform width and depth along strike, equal spacing between faults in the same group) along with their location in the highly active Tharsis volcanic province, enables our interpretation of mapped faults in our study forming as a result from diking (see Shahrzad et al. (2023a) for a description of dike-induced graben formation mechanism). This is contrary to a purely tectonic extension origin, which usually manifests as much larger with fewer grabens over such an area (Fernández & Ramírez-Caballero, 2019; Shahrzad et al., 2023a). This interpretation is also aided by the orientation and locations of collapse features, following the paths of grabens in the groups. This is however not the case for the eastern curved faults in Group 3. These faults are wider spaced, and do not have any collapse features with the graben traces. We therefore reject a dike-origin for these faults and suggest a more purely tectonic origin for the curved Group 3 faults.

4.3. Cavities causing observed collapse structures, originating from diking processes.

We mapped a significant amount of collapse structures in Ceraunius (North and South) and Tractus Fossae. These were pit-crater chains, catenae, u-shaped troughs and chasmatas, which appear in all three study areas. Common for all four features, are their young ages, as all the features crosscut the faulting in the area. We consider the process that may have created them, and the connection to the surrounding faulting and their origins.

Our mapping revealed that the chasmata and u-shaped troughs both show patterns of pit-crater chains when examining the MOLA topography in addition to the CTX images. Combining this with the erosional evolution from pit-crater chains to catenae, we consider the 4 collapse structures as 3-4 steps in the erosional evolution of an initial pit-crater chain (Figure 9a), an evolution initially suggested by Wyrick et al. (2004). This implies a common formation mechanism for them all, which then evolves with time through the different stages, with either a u-shaped trough or a chasmata as the final result.

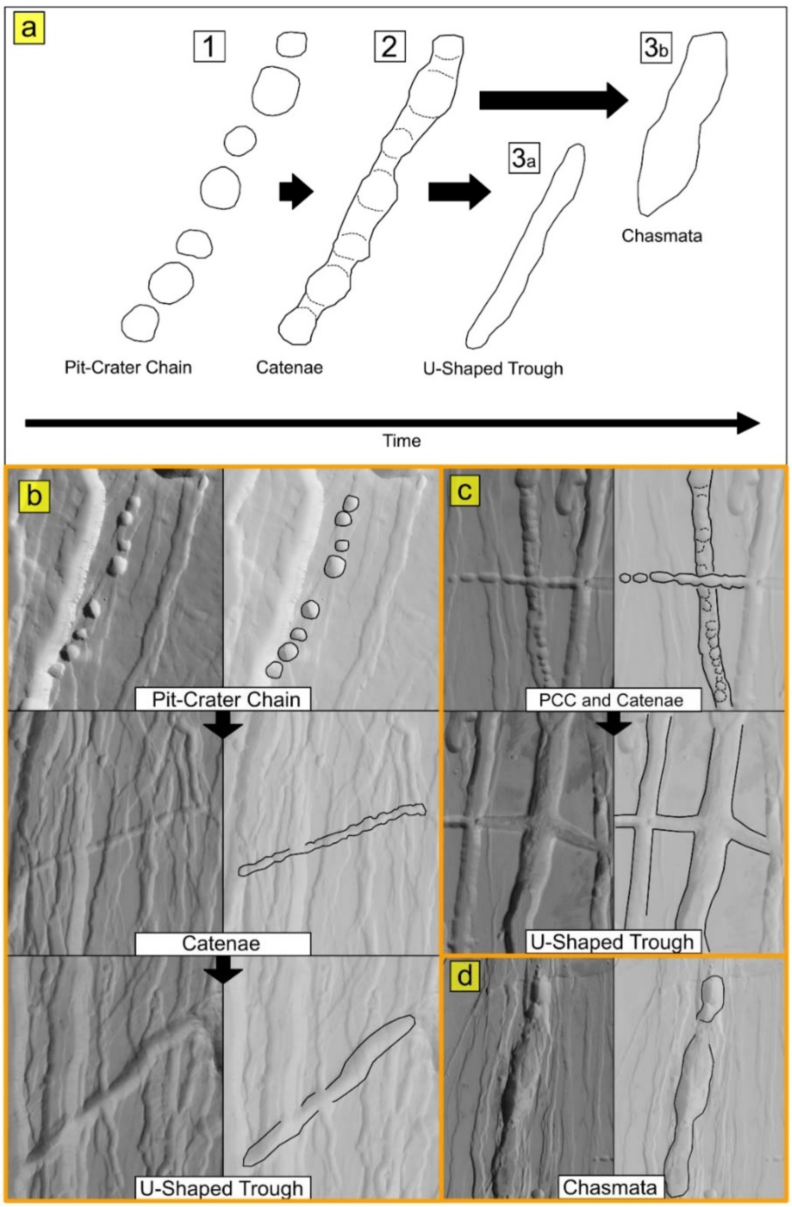

Figure 9: Overview of collapse structure evolution. A) evolution from Pit-crater chain to either U-shaped trough or Chasma. B) Examples of proposed PCC to U-Shaped trough evolution, with CTX image on the left, and interpretation on the right. C) Example of more complex trough development through intersecting PCC and catenae. D) Example of Chasma.

Previously, the collapse features have been explained by a collapse of material into subterranean cavities (Hardy, 2021). It is however still disputed by which mechanism the cavities are created under the Martian surface. There are several proposed origins for cavity formation, with the most common two being 1) cavities due to the rapid withdrawal, or volatile outgassing of magma in a dike (Mège et al., 2003; Scott et al., 2002), and 2) cavities produced by dilational faulting in cohesive material (Ferrill et al., 2011; Wyrick et al., 2004). To explore the feasibility of these origins, we consider our mapped collapse features:

4.3.1. Pit-crater chains and catenae

Similar to Mège et al. (2003), we consider the catenae as an alignment of interacting pit-craters in a chain, and thus consider their formation from the same mechanism (Figure 9a and 9b). Our mapping showed two different types of pit-crater chain and catenae:

The first variety of pit-crater chains (PCCs) and catenae which are found within the mapped grabens, follow their orientation along strike. The second variety of mapped PCCs and catenae do not appear within grabens, but still follow the fault orientations (Figure 8a). The size and shape of the craters are equally variable between the two types, but their orientations differ significantly. The PCCs that follow the exact orientation of the mapped grabens are often located right along the side of a graben-bounding fault (See Figure 8b). These PCCs and catenae all follow the orientations of faults in Group 1, 2, and the linear faults in Group 3 (Table 5).

The remaining mapped PCCs and are not bounded by any faults, yet they still follow the orientations of the fault in Group 1 or 2, either N-S or NNE/SSW. Due to the lack of surface faults or fractures associated with them, we cannot attribute these collapse features to extensional dilation fractures alone, based on the previous criteria (Cushing et al., 2015). We do however still determine them to be diking-induced, though the dikes producing the non-graben bound PCCs and catenae, did not evolve sufficiently in order to induce any surface grabens.

Of the two common PCC formation theories: dike-induced and dilational faulting (E.g. Ferrill et al., 2011; Hardy, 2021; Wyrick et al., 2004), let us consider both theories. As mentioned, the PCCs display fault driven formation characteristics, which would suggest a tectonic origin. While the mapped PCCs are located in large-scale extensional environments, we have determined the source of the extensional faulting in the study area to be largely dike-driven. Dilational faulting is considered a purely tectonic process (Wyrick et al., 2004), where extension in a heterogeneous layered material, allows unconsolidated material to fall into cavities developed in an underlying layer of more competent material. For the diking-related formation, volatile outgassing, magma withdrawal or interactions with the cryosphere from an arrested dike-tip, can produce cavities for the overlying material to collapse into (Scott et al., 2002; Wyrick et al., 2004). Depending on the ascending dike's development, this could occur coeval or post dike-induced graben formation. Both these options would explain the observed PCC formation. As we have determined pervasive diking in the area (i.e., the mapped graben), intense magmatic activity (e.g., small shields and lava flows mapped by Krishnan & Kumar (2023)), we consider it more likely for the formation of the mapped PCCs to be due to or related to the diking in the area. Whether the cavities are a result of dilational faulting produced by the arrested dike tips, or from another process e.g., rapid withdrawal of magma or volatile outgassing, we cannot determine. We do however exclude that our mapped pit-craters are a result of explosive eruptions from the ascending dikes, as we see no evidence of lava flow or eruptions associated directly with the mapped PCCs. As the mapped PCCs are consistently younger than the grabens, we suggest that the PCCs formation is related to later episodes of diking, where the magma has largely followed the paths of the graben-forming dikes. These later episodes may have ascended to an even shallower depth than the previous dikes, and either 1) created further extensional faulting within the wider original grabens, where the path was already weakened, or 2) released the volatiles in the dike, either by ascended to shallow enough depth or due to a more volatile-rich magma, creating the PCCs.

4.3.2. U-shaped troughs and Chasmata

The orientation of the U-shaped troughs varies immensely, with some following the fault pattern and some changing orientation along strike. This may reflect erosion between Type 1 and Type 2 pit-crater chains and catenae, as the example shown in Figure 9c. A recent study of Noctis Labyrinthus found that a volatile-rich layer can facilitate the development from pit-craters to trough structures, specifically by the sublimation of a thermokarst layer (Kling et al., 2021). Further inspection of the mapped u-shaped troughs and chasmata in our study do show few (<5) instances of potential thermokarstic terrain, but they are not pervasive enough to base our interpretation on. The intense erosion that has facilitated the U-shaped troughs and chasmata may then be attributed to the intense magmatic activity forming large and cohesive pit-crater chains, and the elevation of the units compared to the surroundings, having enabled more active erosion of the collapse features on the unit.

We interpret the chasmata as another end member of the PCC and catenae evolution chain, either as a 4th step following u-shaped through formation, or as a 3rd step, following catenae formation, bypassing the u-shaped trough formation (Figure 9a and 9d). This is a result of intense erosional formation as evident by the large structure and evidence of mass-wasting along the interior of the chasmatas. This facilitates the growth of the structure, when the slopes become destabilized and induce landslides, widening the cavity (Mège et al., 2003). The large size (Table 5) of the mapped chasmata could also reflect a larger subsurface cavity than the PCCs, catenae and u-shaped troughs.

4.4. Considering the origin of the mapped fault groups

Assuming dike-related tectonic activity for the majority of our faults, we can thus identify two factors, the stress field the dikes have propagated in, and the source of the magma. As the study areas are located in an extremely large and active volcanic zone, there are a high number of magmatic and stress-field candidates, where we therefore narrow our search.

4.4.1. Regional and local E-W stress trajectories

Our initial approach is to broaden the scope and using a similar method to Shahrzad et al. (2023a), we investigate the graben orientations, and determine if they are radially fanning from any volcanic centres. Mapping out geodesic radial paths from approximate volcanic centres near the study area (Alba Mons, Olympus Mons, the Tharsis Montes, etc.) shows no clear relationship between the mapped faults to a single volcanic center, particularly regarding the most prevalent fault group, Group 2 (Table 2). In a general sense, we can assign the N-S oriented faults in Ceraunius Fossae to lie in a radial orientation to Alba Mons, but this is not the case for the N-S faults in Tractus Fossae, where the closest radial orientation is from Ascraeus Mons (Figure 10). However, considering the lack of pervasive fault orientation and volcanic center relationships, what we have instead, is a lot of interacting stress fields from different orientations. These are both regional and local in scope, and in our study area, they all somehow manage to produce N-S oriented faults structures. This means that there is either a E-W regional extensional field overpowering all other extension orientations, or that the local and the regional stress fields are reinforcing each other.

We therefore reconsider the main N-S (Table 2), orientation of the majority of our faults, and determine the presence of a prevalent regional E-W extension over the entire study area.

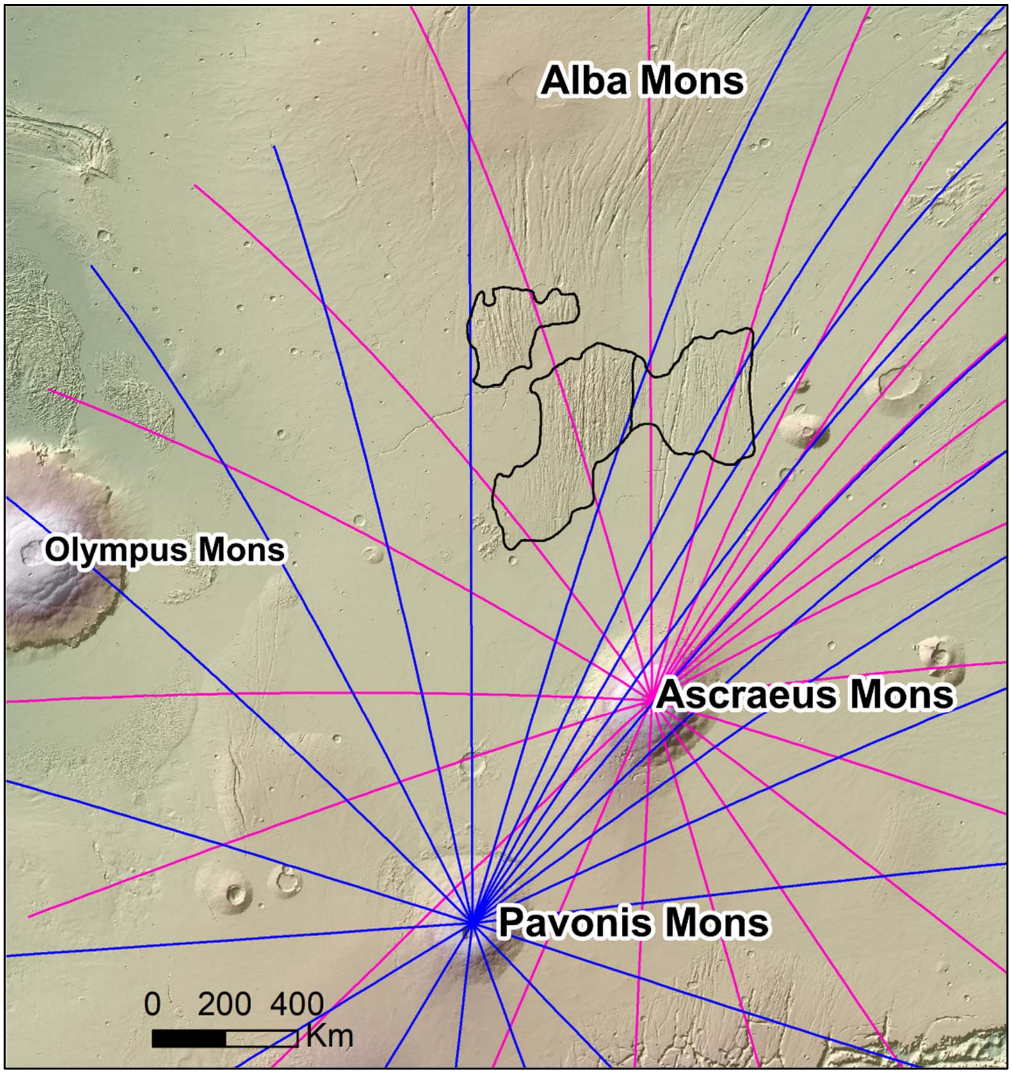

Figure 10: Geodesic radial path orientations from Pavonis Mons and Ascraeus Mons, in relation to mapped study area (black outline).

The source of this E-W extension is likely a reflection of the large-scale regional extension of Tharsis, with potential assistance from any local extension from Alba Mons and Ascraeus Mons (Figure 10). This regional extension has previously been attributed to a regional E-W Tharsis-wide extensional event centered in Syria Planum, located to the south of the study areas (Tanaka, 1990). Here, they determine an evolution of initial isostatic doming producing radial grabens proximal to the deformation center, which is then followed by a period of flexure, producing the distal grabens we see in Ceraunius and Tractus Fossae (Tanaka, 1990). As we consider these features to be dike-related, Syria Planum could be a potential magma source, though we consider a more proximal source, such as Ceraunius Fossae or Alba Mons, more likely.

4.4.2. Magmatic source

With this regional E-W extension in mind, we consider the source of magma for the propagating dikes. Further examining the study area, in the context of the surrounding area, several features can be highlighted. First, both Ceraunius North and Ceraunius South (and to some degree Tractus Fossae), are at an elevated topography to the surrounding lava plains (Figure 11b). Second, Bouguer gravity maps of Mars (Genova et al., 2016) reveals two low density zones within Ceraunius North and South, with the lowest value of -288 mGal, located in Ceraunius North (Figure 11a). Lastly, examining the global crustal thickness map of Mars (Genova et al., 2016), we observe a zone of relatively higher crustal thickness (~20 km thicker) associated with the topographic highs (Figure 11c), where we would otherwise expect a thinning of the crust in an extension zone. Together, along with the mapped dike-related faulting, these observations suggest a zone of magma, located underneath the Ceraunius Fossae area. This magma zone is potentially a plume off-shoot from the Alba Mons plume, or a zone of magmatic underplating. Both instances would be able to produce the vertically propagate dikes we have mapped in this study.

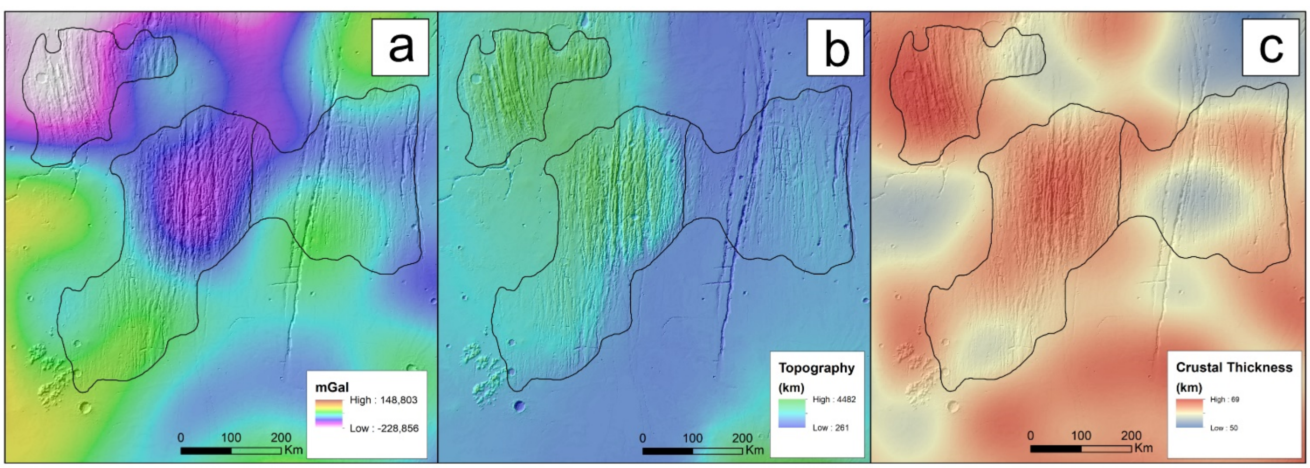

Figure 11: A) Bouguer gravity anomaly map for Mars (centered on study area) from Genova et al. (2006). B) MOLA topographic map of Mars. C) Crustal thickness map of Mars from Genova et al. (2006).

The 2023 study by Krishnan and Kumar, examined boulders, pit-crater chains, lava flows, and select grabens in the Alba Mons area. Their findings conclude that magmatic underplating under Ceraunius Fossae was responsible for the small shield volcanism found in the area, and that the activity of this magma source has been migrating south during the Late Amazonian (Krishnan &

Kumar, 2023). We concur with these findings and expand that the dike-induced faulting mapped in our study is also a result of this magma reservoir. This reservoir is likely an off-shoot or otherwise related to the larger Alba Mons plume (Krishnan & Kumar, 2023; Pieterek et al., 2022). Extension values also support a more directly intense extensional environment immediately above the recognized magma source, with 3.2% extension in Ceraunius South compared to the maximum 1.20% in the NS faults in Tractus Fossae. Considering the orientation of our mapped graben features, we suggest a pattern of vertically propagating dikes, radial above a centralized Ceraunius

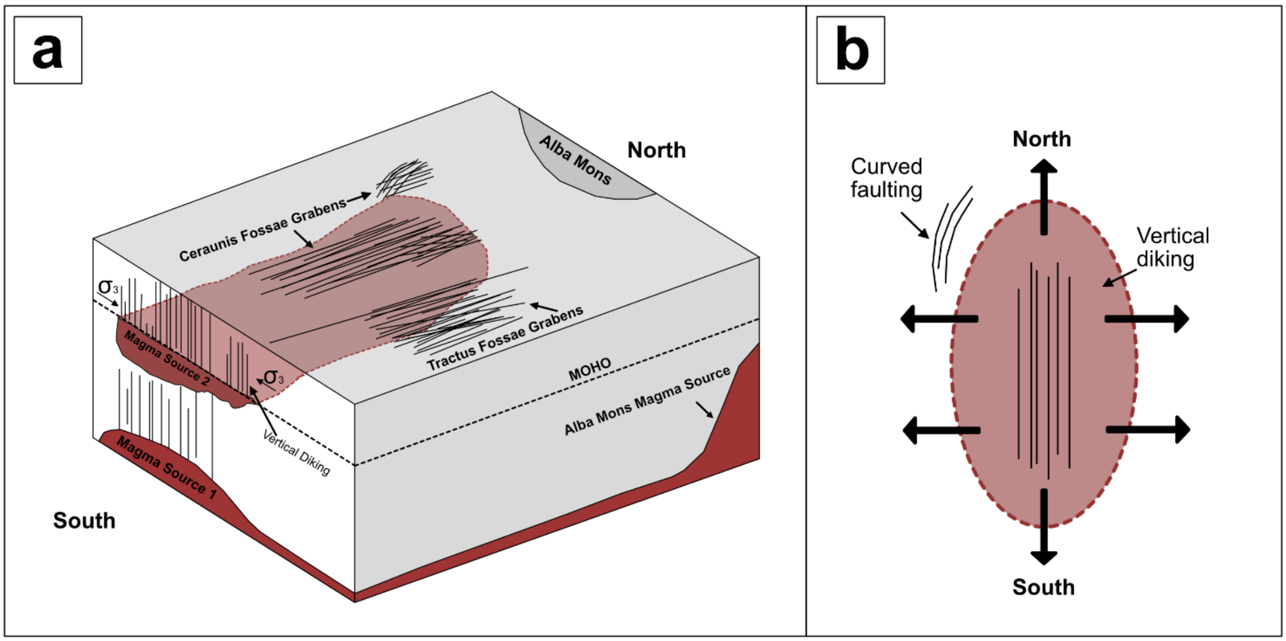

Figure 12: a) Diagram of suggested Ceraunius Fossae magma source. Magma source 1 is the deep source feeding the shallower Magma Source 2, which in this model is magmatic underplating, but could also be a plume off-shoot from an Alba Mons plume. Vertical diking and thus the N-S grabens above the red Magma Source 2 area, is a result of the E-W extension from the magma source, combined with a regional E-W extension. This results in N-S faulting immediately above (Ceraunius North and South) and east (Tractus Fossae) of the supposed Magma Source 2. b) shows a simplified suggestion of the magma source shape, and the surface faults the orientations of extension produced.

Fossae magma source. Figure 12 illustrates a potential Ceraunius Fossae centered magma source, in this case by underplating, as suggested by Krishnan & Kumar (2023).

This would explain the mapped N-S oriented grabens in Ceraunius Fossae but does not entirely justify the dike-induced grabens in Tractus Fossae. Though deformational centres related to magma chambers can vary laterally, for example, with a asymmetric magma chamber (Gudmundsson, 2020), we suggest a combination of E-W radial stresses on the surface above the magma chamber, along with any E-W radial extension fields radiating from the Alba Mons and Ascraeus Mons volcano-tectonic centres, are responsible for the N-S oriented faults in Tractus

Fossae. The overlapping E-W stress fields from Alba Mons, Ascraeus Mons and likely, Syria Planum, reinforced each other and facilitated the vertical diking in Tractus Fossae from a Ceraunius Fossae centered magma source.

4.4.3. Sources of extensional stresses for each fault group

With these theories in mind, we determine the source of extensional stresses for the mapped fault groups.

Group 1: An exact source for the stresses responsible for Group 1 is difficult to determine with certainty, as the combination of location and orientation can result from a number of extensional events. The faults in Group 1 follow an NNE orientation. We have determined the extension to be dike-induced, which corresponds to orientation of the largest collapse features mapped in this study. With this in mind, we consider the orientation of features surrounding Alba Mons. Acheron and Phlegethon Catena are both parallel in orientation to the mapped Group 1 faults, with an NNE/SSW strike. These two Catenae are considered the surface expressions of dikes (Raitala, 1988; Scott et al., 2002). The same is suggested for Tractus Catenae, which we have also identified as a collapse structure in this study, and is determined as dike-induced (Mège et al., 2003). This suggests a correlation between their origins, where the Group 1 faults would be a part of the extensive Tharsis diking, which is radial to the bulge itself (Raitala, 1988). Additionally, we also consider the effect of the more “local” volcanoes, where Group 1 faults have a best fit with projected radial orientations from Pavonis Mons. Early Amazonian Pavonis Mons activity has been recorded (Bouley et al., 2018), which would fit with the expected time of activity for Group 1, and the resulting dikes are a reflection of Tharsis and Pavonis radial stresses.

Group 2: The Ceraunius Fossae part of Group 2 grabens (Figure 5) are the result of vertical diking, likely from a local plume or magmatic underplating source (Figure 12a). For reasons discussed above, Tractus Fossae appears different as it lacks the evidence of a low-density anomaly underneath and is thus not considered to be located directly above the magma source. The extensive N-S diking in Group 2, is likely the result of several interacting stress fields, namely the regional Tharsis E-W extension, and E-W extension related to Alba Mons and Ascraeus Mons, though we still consider an Alba Mons plume, or the potential Ceraunius Fossae underplating, the source of the dikes, with the surrounding extensions explaining the dike orientations.

A highlighted feature of this group is the high density of faulting (Figure 4c) in Ceraunius South. We consider it a likely overprinting of several stages of largely NS oriented faulting, which are near-impossible to distinguish from each other.

Group 3: The majority of the faults mapped in this group are in Ceraunius North, and it contains both linear and a portion of curved faults. Curved faults are found in several places on Mars, such as Alba Fossae around Alba Mons (Öhman & McGovern, 2014), and around other volcanoes such as Labeatis Mons (Orlov et al., 2022). Common for these, is that the structures all curve around a volcanic center, which is not the case for the northern Group 3 faults. As discussed above, we do not consider these faults dike related. Additionally, none of the mapped collapse features follow the orientation of the faults in Group 3, lending to their non-dike origin. As there are no signs of a buried volcanic structure near the faults, we consider their origin a more likely result from interacting stress fields. However, instead of reinforcing each other, as in the case with Tractus Fossae, they change the orientation of the structure. Figure 12b shows a suggestion on how this may occur. Here we assume an elongated magma source, where the bounding extensional stresses results in curved grabens. Curved grabens are also indicative of either loading or deflation associated with a volcanic center (Cailleau et al., 2003a; Mège & Masson, 1996). As mentioned, we do not observe any structure the faults would be circumferential to, but deflation of a volcanic center (e.g., by cooling or magma withdrawal), which was then covered by more recent lava flows, remains another possibility. Additional modelling of the proposed Ceraunius Fossae magma source would be needed to confirm this.

The linear NNW trending faults in this group have collapse features in the same orientation, and within the grabens, and their radial orientation to the nearby Ascraeus Mons suggests diking related activity as the source of these faults. The linear and curved faults appear side-by-side, so their slight change in orientation cannot be distinguished temporally between the two.

4.5. Stages of deformation south of Alba Mons.

We have identified four main stages of structural activity in Ceraunius Fossae and Tractus Fossae, all occurring in the Amazonian. Based on their ages and orientation we propose the following stages of evolution of the southern area of Alba Mons (Figure 13).

1. Following an Amazonian lava emplacement, laterally propagating radial dikes from a volcanotectonic center near the mid of the Tharsis bulge reflect the first recorded extension

activity in Ceraunius South and Tractus Fossae. NNW-SSE extension facilitates NNE trending faults in Tractus Fossae and Ceraunius South (Figure 13a). These diking induced grabens are likely sourced from either Pavonis Mons or Tharsis itself.

2. Previous regional E-W extension related to the isostatic loading of Syria Planum, has likely weakened the crust is Ceraunius Fossae and Tractus Fossae, and thus aided the emergence of Alba Mons plume/Ceraunius Fossae underplating sourced vertical diking-induced faulting (Figure 13b). This E-W extension that allowed the intensity of the N-S faulting, was likely amplified by radial stresses from Alba Mons and Ascraeus Mons.
3. Activity from the Ceraunius Fossae magma source, perhaps related to late-stage deflation in accordance with diminishing activity, creates a set of curved faults to the south of Alba Mons (Figure 13c).
4. Any low-lying lands are covered with the most recent Amazonian lava flows, isolating the raised patches we map in this study (Figure 13d).

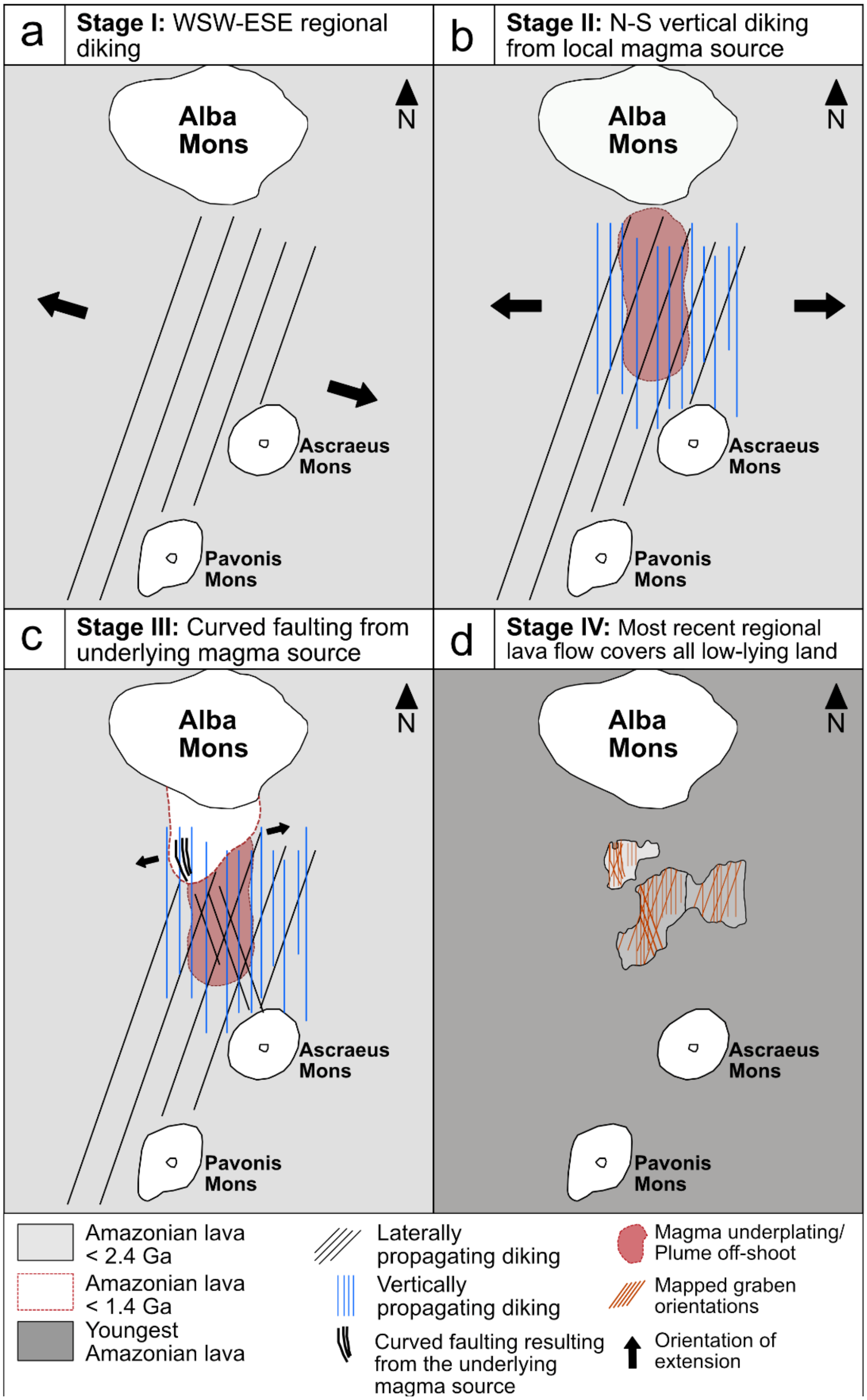

Figure 13: The 4 main stages of tectonic activity in the southern Alba Mons, all occurring during the Amazonian. A) Stage I, initial NNW/SSE extension, due to Tharsis bulge centered diking. Results in NNE oriented grabens. B) Stage II, activity from Ceraunius Fossae centered magma source, combined with regional (Syria Planum centered) and local (Alba Mons and Ascraeus Mons) E-W extension produces N-S oriented vertical diking. C) Stage III, interacting stress fields from the Ceraunius Fossae magma source, together with Ascraeus Mons diking produces linear and curved faulting. D) The most recent Amazonian lava flow covers all low-lying terrain.

4.6. Implications for magma reservoir location

Results from the fault mapping and grouping reveals 3 main stages of extensional activity in Ceraunius and Tractus Fossae, occurring during the Amazonian. Overall, the area south of Alba Mons show intense surface deformation, the majority of which is associated with the magmatic activity localized here. We observe extensional faulting as a result of diking, and collapse features such as pit-crater chains, which we consider the result of arrested dikes interacting with the surface. As mentioned, the magma that fed the extensive diking and subsequent extensional faulting and collapse structures around the surface of Alba Mons, is suggested to originate from a separate source, independent from the Tharsis superplume.

Other highly faulted volcanotectonic areas such as Ulysses Fossae (Fernández & Ramírez-Caballero, 2019; Shahrzad et al., 2023a) and Noctis Labyrinthus (Kling et al., 2021), display similar pit-crater chain and catenae morphology as the ones we have mapped south of Alba Mons. The complexity of troughs however varies between the three locations on a range. Ulysses Fossae has only a few contained compound trough structures in UF North (Shahrzad et al., 2023a), Alba Mons is more developed with the u-shaped troughs and chasmatas mapped in this study, and then the intricate chaotic terrain and interacting troughs in Noctis Labyrinthus define the majority of the structures there (Kling et al., 2021).

Particular for the Alba Mons hotspot, a 2006 study concluded that the magma reservoir feeding the Alba Mons lobes must be located at a relatively shallow depth (high topographic level), compared to other Tharsis volcanoes (Ivanov & Head, 2006). Additionally, Mège et al. (2003), investigated representative areas of Alba Patera and Noctis Labyrinthus, and found that magma reservoirs might lie at ~1 km and ~5 km depth respectively. These findings could indicate that the source of magma was relatively close to the surface, compared to the rest of the Tharsis volcanoes and could thus have an influence on the amount and longevity of the diking, and the subsequent high-density faulting and collapse structures. Other Tharsis volcanoes such as the Tharsis Montes show pit-crater chain structures on the flanks of the volcanoes, but given the distance from the main volcano for the faults in Noctis Labyrinthus (Kling et al., 2021) and Ceraunius- and Tractus Fossae, a relatively more shallow magma source (and near-surface volatile layers) could be the reason for the complexity of the collapse structures in those locations, compared to Ulysses Fossae (Shahrzad et al., 2023a). There, the comparative "lack" of complex collapse features from the majority of the Tharsis-superplume related volcanoes, could reflect a deeper magma source.

However, this is just one possible explanation and further modelling of the potential magmatic reservoirs are necessary to confirm or refute it.

5 Conclusions

- In this study we mapped and measured ~12,000 faults and determined their ages of activity based on crater size-frequency distributed ages, as being active during the Amazonian period, late in Mars' history.
- Grouping the faults based on orientation and morphology reveals 3 distinct stages of extensional activity recorded in the study areas, with a temporal change from NE to NS to NW oriented faults and associated perpendicular extensional strain orientations.
- We determine the majority of the faulting to be dike-induced (Groups 1, 2 and some of 3), with both regional (Tharsis) and local (Alba Mons, Ascraeus Mons and Pavonis Mons) centres of deformation. We determine the curved western faults in Group 3 to be purely tectonic and a result of the stresses from a local magmatic source.
- Additionally, the mapped collapse structures are also considered related to diking and are consistently younger than the mapped faults.
- The magmatic activity from a local Ceraunius Fossae magma source (either from an Alba Mons plume off-shoot, or magmatic underplating), has highly influenced Ceraunius and Tractus Fossae, with dike-induced graben formation and associated pit-crater chains, catenae, u-shaped troughs and chasmatas dotting the landscape. This potentially shallow and recent (< 1.4 Ga) magmatic activity was inducive to the mapped surface deformation, which was amplified by the regional Tharsis E-W extension, with influence from radial stresses from local volcanoes.

6 Data Availability Statement

Mapped faults, collapse features, and craters from this study are available to download free from Zenodo: faults (Shahrzad, 2023b), collapse features (Shahrzad, 2023c), craters (Shahrzad, 2023d). The CTX images (Malin et al., 2007) used in this study can be downloaded from NASA's PDS Geoscience Node at https://pds-imaging.jpl.nasa.gov/portal/mro_mission.html and the MOLA-HRSC DEM v2 used to generate topographic profiles is available from USGS' Astropedia Catalog (Fergason et al., 2018). The software used in this research is available to download for free: Craterstats 2.0 is available from the Freie Universität Berlin at https://www.geo.fu-berlin.de/en/geol/fachrichtungen/planet/software/index.html and FracPaQ (Healy et al., 2017) is available for download via GitHub.

7 References

Banerdt, W. B., Golombek, M. P., & Tanaka, K. L. (1992). Stress and tectonics on Mars. In *Mars* (pp. 249–297). https://ui.adsabs.harvard.edu/abs/1992mars.book..249B

Belleguic, V., Lognonné, P., & Wieczorek, M. (2005). Constraints on the Martian lithosphere from gravity and topography data. *Journal of Geophysical Research: Planets*, *110*(E11). https://doi.org/10.1029/2005JE002437

Bouley, S., Baratoux, D., Matsuyama, I., Forget, F., Séjourné, A., Turbet, M., & Costard, F. (2016). Late Tharsis formation and implications for early Mars. *Nature*, *531*(7594), 344–347. https://doi.org/10.1038/nature17171

Bouley, S., Baratoux, D., Paulien, N., Missenard, Y., & Saint-Bézar, B. (2018). The revised tectonic history of Tharsis. *Earth and Planetary Science Letters*, *488*, 126–133. https://doi.org/10.1016/j.epsl.2018.02.019

Byrne, P. K., Holohan, E. P., Kervyn, M., van Wyk de Vries, B., & Troll, V. R. (2015). Analogue modelling of volcano flank terrace formation on Mars. *Geological Society, London, Special Publications*, *401*(1), 185–202. https://doi.org/10.1144/SP401.14

Cailleau, B., Walter, T. R., Janle, P., & Hauber, E. (2003a). Modeling volcanic deformation in a regional stress field: Implications for the formation of graben structures on Alba Patera, Mars. *Journal of Geophysical Research: Planets*, *108*(E12). https://doi.org/10.1029/2003JE002135

Cailleau, B., Walter, T. R., Janle, P., & Hauber, E. (2003b). Modeling volcanic deformation in a regional stress field: Implications for the formation of graben structures on Alba Patera, Mars. *Journal of Geophysical Research: Planets*, *108*(E12). https://doi.org/10.1029/2003JE002135

Cailleau, B., Walter, T. R., Janle, P., & Hauber, E. (2005). Unveiling the origin of radial grabens on Alba Patera volcano by finite element modelling. *Icarus*, *176*(1), 44–56. https://doi.org/10.1016/j.icarus.2005.01.017

Carr, M. H. (1974). Tectonism and volcanism of the Tharsis Region of Mars. *Journal of Geophysical Research (1896-1977)*, *79*(26), 3943–3949. https://doi.org/10.1029/JB079i026p03943

Christoph, J. M., & Garry, W. B. (2017). *Spatial and Temporal Relationships Among Low Shield Volcanoes in the Ceraunius Fossae Region of Tharsis: The Last Gasp of Martian Volcanism*. 2798.

Cushing, G. E., Okubo, C. H., & Titus, T. N. (2015). Atypical pit craters on Mars: New insights from THEMIS, CTX, and HiRISE observations. *Journal of Geophysical Research: Planets*, *120*(6), 1023–1043. https://doi.org/10.1002/2014JE004735

Dohm, J. M., Baker, V. R., Maruyama, S., & Anderson, R. C. (2007). Traits and Evolution of the Tharsis Superplume, Mars. In D. A. Yuen, S. Maruyama, S.-I. Karato, & B. F. Windley (Eds.), *Superplumes:*

Beyond Plate Tectonics (pp. 523–536). Springer Netherlands. https://doi.org/10.1007/978-1-4020-5750-2_17

Fergason, R. L., Hare, T. M., & Laura, J. (2018). *HRSC and MOLA Blended Digital Elevation Model at 200m v2.* [Map]. Astrogeology PDS Annex, U.S. Geological Survey.

Fernández, C., & Ramírez-Caballero, I. (2019). Evaluating transtension on Mars: The case of Ulysses Fossae, Tharsis. *Journal of Structural Geology*, *125*, 325–333. https://doi.org/10.1016/j.jsg.2018.05.009

Ferrill, D. A., Wyrick, D. Y., & Smart, K. J. (2011). Coseismic, dilational-fault and extension-fracture related pit chain formation in Iceland: Analog for pit chains on Mars. *Lithosphere*, *3*(2), 133–142. https://doi.org/10.1130/L123.1

Genova, A., Goossens, S., Lemoine, F. G., Mazarico, E., Neumann, G. A., Smith, D. E., & Zuber, M. T. (2016). Seasonal and static gravity field of Mars from MGS, Mars Odyssey and MRO radio science. *Icarus*, *272*, 228–245. https://doi.org/10.1016/j.icarus.2016.02.050

Gudmundsson, A. (2020). *Volcanotectonics—Understanding the Structure, Deformation and Dynamics of Volcanoes*. https://doi.org/10.1017/9781139176217

Hardy, S. (2021). Discrete Element Modelling of Pit Crater Formation on Mars. *Geosciences*, *11*(7), Article 7. https://doi.org/10.3390/geosciences11070268

Healy, D., Rizzo, R. E., Cornwell, D. G., Farrell, N. J. C., Watkins, H., Timms, N. E., Gomez-Rivas, E., & Smith, M. (2017). FracPaQ: A MATLAB™ toolbox for the quantification of fracture patterns. *Journal of Structural Geology*, *95*, 1–16. https://doi.org/10.1016/j.jsg.2016.12.003

Ivanov, M. A., & Head, J. W. (2006a). Alba Patera, Mars: Topography, structure, and evolution of a unique late Hesperian–early Amazonian shield volcano. *Journal of Geophysical Research: Planets*, *111*(E9). https://doi.org/10.1029/2005JE002469

Ivanov, M. A., & Head, J. W. (2006b). Alba Patera, Mars: Topography, structure, and evolution of a unique late Hesperian–early Amazonian shield volcano. *Journal of Geophysical Research: Planets*, *111*(E9). https://doi.org/10.1029/2005JE002469

Jenness, J. (2011). Tools for Graphics and Shapes. *Jenness Enterprises*.

Kling, C. L., Byrne, P. K., Atkins, R. M., & Wegmann, K. W. (2021). Tectonic Deformation and Volatile Loss in the Formation of Noctis Labyrinthus, Mars. *Journal of Geophysical Research: Planets*, *126*(11), e2020JE006555. https://doi.org/10.1029/2020JE006555

Kneissl, T., van Gasselt, S., & Neukum, G. (2011). Map-projection-independent crater size-frequency determination in GIS environments—New software tool for ArcGIS. *Planetary and Space Science*, *59*(11), 1243–1254. https://doi.org/10.1016/j.pss.2010.03.015

Krishnan, V., & Kumar, P. S. (2023). Long-Lived and Continual Volcanic Eruptions, Tectonic Activity, Pit Chains Formation, and Boulder Avalanches in Northern Tharsis Region: Implications for Late Amazonian Geodynamics and Seismo-Tectonic Processes on Mars. *Journal of Geophysical Research: Planets*, *128*(1), e2022JE007511. https://doi.org/10.1029/2022JE007511

Malin, M. C., Bell, J. F., Cantor, B. A., Caplinger, M. A., Calvin, W. M., Clancy, R. T., Edgett, K. S., Edwards, L., Haberle, R. M., James, P. B., Lee, S. W., Ravine, M. A., Thomas, P. C., & Wolff, M. J. (2007). Context Camera Investigation on board the Mars Reconnaissance Orbiter. *Journal of Geophysical Research: Planets*, *112*(E5). https://doi.org/10.1029/2006JE002808

Mège, D. (1999). *Dikes on Mars: (1) What to Look For? (2) A First Survey of Possible Dikes During the Mars Global Surveyor Aerobreaking and Science Phasing Orbits* (p. 6207). https://ui.adsabs.harvard.edu/abs/1999ficm.conf.6207M

Mège, D., Cook, A. C., Garel, E., Lagabrielle, Y., & Cormier, M.-H. (2003). Volcanic rifting at Martian grabens. *Journal of Geophysical Research: Planets*, *108*(E5). https://doi.org/10.1029/2002JE001852

Mège, D., Cook, A., Garel, E., Lagabrielle, Y., & Cormier, M.-H. (2002). *Surface Collapse and Volcanic Rifting on Mars*. *33*, 2042.

Mège, D., & Masson, P. (1996). A plume tectonics model for the Tharsis province, Mars. *Planetary and Space Science*, *44*(12), 1499–1546. https://doi.org/10.1016/S0032-0633(96)00113-4

Michael, G. G. (2013). Planetary surface dating from crater size–frequency distribution measurements: Multiple resurfacing episodes and differential isochron fitting. *Icarus*, *226*(1), 885–890. https://doi.org/10.1016/j.icarus.2013.07.004

Michael, G. G., Kneissl, T., & Neesemann, A. (2016). Planetary surface dating from crater size-frequency distribution measurements: Poisson timing analysis. *Icarus*, *277*, 279–285. https://doi.org/10.1016/j.icarus.2016.05.019

Öhman, T., & McGovern, P. J. (2014). Circumferential graben and the structural evolution of Alba Mons, Mars. *Icarus*, *233*, 114–125. https://doi.org/10.1016/j.icarus.2014.01.043

Orlov, C. J., Bramham, E. K., Thomas, M., Byrne, P. K., Piazolo, S., & Mortimer, E. (2022). Structural Architecture and Deformation History of Tempe Terra, Mars. *Journal of Geophysical Research: Planets*, *127*(11), e2022JE007407. https://doi.org/10.1029/2022JE007407

Pieterek, B., Ciazela, J., Lagain, A., & Ciazela, M. (2022). Late Amazonian dike-fed distributed volcanism in the Tharsis volcanic province on Mars. *Icarus*, *386*, 115151. https://doi.org/10.1016/j.icarus.2022.115151

Plescia, J. B. (2004). Morphometric properties of Martian volcanoes. *Journal of Geophysical Research: Planets*, *109*(E3). https://doi.org/10.1029/2002JE002031

Polit, A. T., Schultz, R. A., & Soliva, R. (2009). Geometry, displacement–length scaling, and extensional strain of normal faults on Mars with inferences on mechanical stratigraphy of the Martian crust. *Journal of Structural Geology*, *31*(7), 662–673. https://doi.org/10.1016/j.jsg.2009.03.016

Raitala, J. (1988). Composite graben tectonics of Alba Patera on Mars. *Earth, Moon, and Planets*, *42*(3), 277–291. https://doi.org/10.1007/BF00058491

Scott, E. D., Wilson, L., & Head III, J. W. (2002). Emplacement of giant radial dikes in the northern Tharsis region of Mars. *Journal of Geophysical Research: Planets*, *107*(E4), 3-1-3–10. https://doi.org/10.1029/2000JE001431

Shahrzad, S., Bramham, E. K., Thomas, M., Piazolo, S., Byrne, P. K., & Mortimer, E. (2023a). Deciphering the Structural History of Ulysses Fossae, Mars, Using Fault Pattern Analysis. *Journal of Geophysical Research: Planets*, *128*(5), e2022JE007633. https://doi.org/10.1029/2022JE007633

Shahrzad, S. (2023b). Ceraunius Fossae and Tractus Fossae fault catalogue [Dataset]. Zenodo. https://doi.org/10.5281/zenodo.8376744

Shahrzad, S. (2023c). Ceraunius Fossae and Tractus Fossae crater catalogue [Dataset]. Zenodo. https://doi.org/10.5281/zenodo.8376774

Shahrzad, S. (2023d). Ceraunius Fossae and Tractus Fossae collapse features catalogue [Dataset]. Zenodo https://doi.org/10.5281/zenodo.8376769

Stubblefield, R. K. (2018). *Extensional Tectonics at Alba Mons, Mars: A Case Study for Local versus Regional Stress Fields.* [Master of Science, North Carolina State University]. http://www.lib.ncsu.edu/resolver/1840.20/36604

Tanaka, K. L. (1990). Tectonic history of the Alba Patera—Ceraunius Fossae region of Mars. *Lunar and Planetary Science Conference Proceedings*, *20*, 515–523.

Tanaka, K. L., Golombek, M. P., & Banerdt, W. B. (1991). Reconciliation of stress and structural histories of the Tharsis region of Mars. *Journal of Geophysical Research: Planets*, *96*(E1), 15617–15633. https://doi.org/10.1029/91JE01194

Tanaka, K. L., Skinner Jr., J. A., Dohm, J. M., Irwin, III, R. P., Kolb, E. J., Fortezzo, C. M., Platz, T., Michael, G. G., & Hare, T. M. (2014). *Geologic Map of Mars* (Scientific Investigations Map) [Scientific Investigations Map].

Wyrick, D., Ferrill, D. A., Morris, A. P., Colton, S. L., & Sims, D. W. (2004). Distribution, morphology, and origins of Martian pit crater chains. *Journal of Geophysical Research: Planets*, *109*(E6). https://doi.org/10.1029/2004JE002240